Short Article

Molecular Cell

The Immune Adaptor SLP-76 Binds to SUMO-RANGAP1 at Nuclear Pore Complex Filaments to Regulate Nuclear Import of Transcription Factors in T Cells

Graphical Abstract

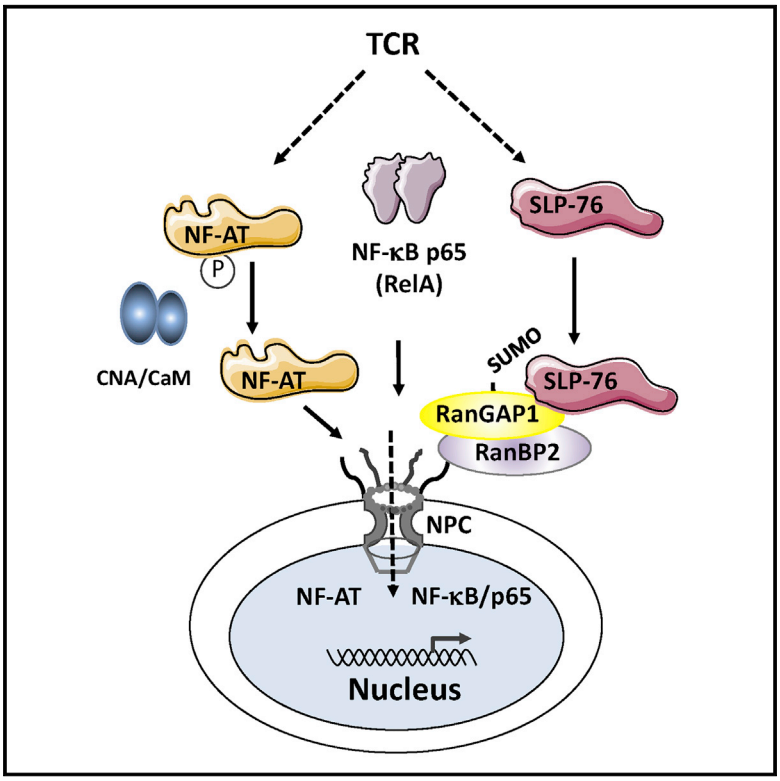

Authors

Hebin Liu, Helga Schneider, Asha Recino, Christine Richardson, Martin W. Goldberg, Christopher E. Rudd

Correspondence

cer51@cam.ac.uk

In Brief

Liu et al. show that the direct binding of the immune cell adaptor SLP-76 to SUMO-RanGAP1 of cytoplasmic fibrils of the nuclear pore complex (NPC) is needed for the optimal NFAT and NFkB nuclear entry in T cells.

Highlights

- Immune adaptor SLP-76 binds to SUMO-RanGAP1 of cytoplasmic fibrils of the NPC
- SLP-76 K-56 binding needed for optimal RanGAP1 localization and exchange activity
- SLP-76 K56E mutant impaired NF-ATc1 and NFκB p65 (RelA) nuclear entry
- Immune adaptors directly regulate nuclear entry of transcription factors in T cells

Liu et al., 2015, Molecular Cell *59*, 840–849
September 3, 2015
http://dx.doi.org/10.1016/j.molcel.2015.07.015

CellPress

Molecular Cell
Short Article

The Immune Adaptor SLP-76 Binds to SUMO-RANGAP1 at Nuclear Pore Complex Filaments to Regulate Nuclear Import of Transcription Factors in T Cells

Hebin Liu,[1,3] Helga Schneider,[1] Asha Recino,[1] Christine Richardson,[2] Martin W. Goldberg,[2] and Christopher E. Rudd[1,*]
[1]Cell Signaling Section, Department of Pathology, University of Cambridge, Tennis Court Road, Cambridge CB2 1QP, UK
[2]School of Biological and Biomedical Sciences, Durham University, Science Laboratories, South Road, Durham DH1 3LE, UK
[3]Present address: Department of Biological Sciences, Xi'an Jiaotong-Liverpool University, 111 Renai Road, SIP Suzhou, Jiangsu Province 215123, China
*Correspondence: cer51@cam.ac.uk
http://dx.doi.org/10.1016/j.molcel.2015.07.015

SUMMARY

While immune cell adaptors regulate proximal T cell signaling, direct regulation of the nuclear pore complex (NPC) has not been reported. NPC has cytoplasmic filaments composed of RanGAP1 and RanBP2 with the potential to interact with cytoplasmic mediators. Here, we show that the immune cell adaptor SLP-76 binds directly to SUMO-RanGAP1 of cytoplasmic fibrils of the NPC, and that this interaction is needed for optimal NFATc1 and NF-κB p65 nuclear entry in T cells. Transmission electron microscopy showed anti-SLP-76 cytoplasmic labeling of the majority of NPCs in anti-CD3 activated T cells. Further, SUMO-RanGAP1 bound to the N-terminal lysine 56 of SLP-76 where the interaction was needed for optimal RanGAP1-NPC localization and GAP exchange activity. While the SLP-76-RanGAP1 (K56E) mutant had no effect on proximal signaling, it impaired NF-ATc1 and p65/RelA nuclear entry and in vivo responses to OVA peptide. Overall, we have identified SLP-76 as a direct regulator of nuclear pore function in T cells.

INTRODUCTION

T cells express protein-tyrosine kinases and adaptors that integrate signals for T cell activation (Rudd, 1999; Rudd et al., 2010; Samelson, 2002; Smith-Garvin et al., 2009). Adaptors possess binding sites and discrete modular domains that integrate signals. Immune cell adaptors include SH2 domain containing leukocyte protein of 76 kDa (SLP-76) (Jackman et al., 1995; Smith-Garvin et al., 2009), linker for the activation of T cells (LAT) (Zhang et al., 1998), and adhesion- and degranulation-promoting adaptor protein (ADAP) (da Silva et al., 1997; Liu et al., 1998; Musci et al., 1997). SLP-76 has a N-terminal sterile-α motif (SAM), tyrosine motifs and a SH2 domain and is needed for T cell differentiation and function (Jackman et al., 1995; Jordan et al., 2003; Pivniouk et al., 1998). SLP-76-deficient T cells show an impaired phospholipase Cγ1 (PLCγ1) activation and calcium mobilization (Yablonski et al., 1998), while N-terminal residues are phosphorylated by ZAP-70 (Bubeck Wardenburg et al., 1996; Raab et al., 1997). Y-113 and Y-128 bind exchange factor Vav1 and adaptor Nck (Bubeck Wardenburg et al., 1998; Jackman et al., 1995; Wu et al., 1996), resting lymphocyte kinase (Rlk) (Schneider et al., 2000), and inducible tyrosine kinase (Itk) (Bunnell et al., 2000). SLP-76 binds to the SH3 domain of PLCγ1 (Grasis et al., 2010; Yablonski et al., 2001), while GADs SH2 domain forms a complex with LAT (Zhang et al., 1998). SLP-76 also forms microclusters (Bunnell et al., 2002; Yokosuka et al., 2005), exerts feedback control on ZAP-70 (Liu et al., 2010), and interacts with subsynaptic LAT clusters (Purbhoo et al., 2010; Williamson et al., 2011). The SLP-76 SH2 domain binds to ADAP (da Silva et al., 1997; Musci et al., 1997) and hematopoietic progenitor kinase-1 (HPK-1) (Di Bartolo et al., 2007; Shui et al., 2007). In turn, ADAP binds to adaptor SKAP1 (SKAP-55) for integrin adhesion (Raab et al., 2010, 2011; Wang and Rudd, 2008).

SLP-76 is also needed downstream to activate transcription factors NFAT (nuclear factor for the activation of T cells) and NF-κB (nuclear factor kappa-light-chain-enhancer of activated B cells) (Yablonski et al., 1998). NFAT possesses two basic nuclear localization sequences (NLSs) for nuclear import dependent on dephosphorylation by calcineurin (Müller and Rao, 2010; Wu et al., 2007). Dephosphorylation unmasks nuclear-location signals (Shibasaki et al., 1996). Similarly, NF-κB plays roles in inflammation, cell activation, and differentiation (Ghosh and Karin, 2002; Sen, 2011). Coreceptor CD28 and innate receptors activate NF-κB transcription via different pathways in T cells (Marinari et al., 2002; Thaker et al., 2015).

Nuclear transport is mediated by the nuclear pore complex (NPC) (Chatel and Fahrenkrog, 2012; Hoelz et al., 2011). The NPC is composed of more than 30 nucleoporins (Nups) needed for anchorage and the formation of a central mesh in the channel (Allen et al., 2008; D'Angelo and Hetzer, 2008). Intriguingly, eight filaments extend into the cytoplasm comprised of RanBP2 (Nup358) and RanGAP1, the latter having GTPase activity for GTP-Ran (Bischoff et al., 1994). This interaction requires the ATP-dependent posttranslational conjugation of RanGAP1 with

SUMO-1 (for small ubiquitin-related modifier) (Lee et al., 1998; Mahajan et al., 1997). Ran binding to GTP causes importins to release protein in the nucleus, while nonhydrolysable GTP accumulates Ran-GTP at the filaments (Melchior et al., 1995). RanBP2/RanGAP1 and associated SUMO1/Ubc9 form a multisubunit SUMO E3 ligase (Pichler et al., 2002; Werner et al., 2012).

SLP-76 microclusters at the cell surface translocate to the perinuclear region of T cells (Bunnell et al., 2002). While adaptors mediate TCR proximal signaling, direct regulation of the NPC has not been reported. Here, we show that direct SLP-76 binding to the SUMO-RanGAP1 of cytoplasmic filaments of the NPC is required for the regulation of transcription factor entry into the nucleus of T cells. Our findings identify a surprising direct mechanism of NPC regulation by an immune adaptor in T cells.

RESULTS

SLP-76 Localizes to the Nuclear Pore and Binds to SUMO-RanGAP1

NPC fibrils could potentially interact with cytoplasmic signaling proteins in T cells. Mouse DC27.10 T cells were anti-CD3 ligated for 10 min and imaged by confocal fluorescence microscopy (Figure 1A). Monoclonal antibody to NPC proteins (Mab414) and anti-RanGAP1 stained the nuclear envelop around the DAPI-stained nucleus (upper and middle panels). Anti-CD3-induced endogenous SLP-76 microclusters overlapped with RanGAP1 as detected by antibody staining (middle panel; right expanded image). Immune-gold transmission electron microscopy (TEM) using anti-SLP-76 showed labeling of the cytoplasmic site of the NPC in response to anti-CD3 ligation (lower left versus right panel). Quantitation showed that anti-SLP-76 stained 13% of randomly selected NPCs with gold particles in resting cells (n = 44) (Figure 1B). Remarkably, 76% of NPCs had at least one gold particle within a distance of 130 nm from the cytoplasmic ring in response to anti-CD3 ligation, (i.e., an average of 0.84 particles per NPC of 100 randomly selected NPCs with zero to three labels each). A total of 77% of labels were cytoplasmic (n = 109), with an average distance of ~35 nm from the cytoplasmic ring, a distance comparable to RanGAP staining (histogram).

NPC cytoplasmic fibrils are comprised of RanBP2 and RanGAP1 (Hutten et al., 2008). RanGAP1 exists as a nonsumoylated 70 Kd and a 90 Kd sumoylated form that associates with that NPC (Bernier-Villamor et al., 2002; Matunis et al., 1996). Anti-SLP-76 coprecipitated a 90 Kd protein from mouse DC27.10 T cells and preactivated human primary T cells as recognized by anti-RanGAP1 blotting (Figure 1C, left panel, lanes 2 and 3, and 4 and 5, respectively). Anti-CD3 ligation increased coprecipitated RanGAP1 (upper panel, lane 3 versus lane 2 and lane 5 versus lane 4). Occasionally, a smaller amount of nonsumoylated RanGAP1 was apparent in the anti-SLP-76 precipitates (3/16 experiments). Specificity was shown by the failure of anti-SKAP1 (right panel, lanes 5 and 6), anti-ADAP (lanes 7 and 8), or anti-CARMA1 (lanes 9 and 10) to coprecipitate RanGAP1. A time course showed that the optimal coprecipitation of RanGAP1 was a relatively late event with maximal levels at 10–20 min following anti-CD3 ligation (Figure 1D). Anti-SUMO blotting confirmed that SUMO-RanGAP1 at 90 KD was coprecipitated with anti-SLP-76 over the time course (lower panel). SUMO-RanGAP1 selectively associates with the fibrils of the NPC (Mahajan et al., 1997).

By contrast, anti-SLP-76 failed to precipitate RanBP2 (Nup358) from anti-CD3 activated Jurkat T cells (Figure 1E, upper panel, lanes 3 and 4), while it coprecipitated SUMO-RanGAP1 (lower panel, lanes 3 and 4). Anti-RanGAP1 precipitated itself (lower panel, lanes 1 and 2) and RanBP2 (upper panel, lanes 1 and 2). Similarly, anti-RanGAP1 coprecipitated SLP-76 from 293 T cells transfected with the adaptor (see Figure S1A available online, upper panel, lane 2 versus lane 1). By contrast, anti-RanBP2 failed to coprecipitate SLP-76 from 293 T cells expressing RanBP2 plus SLP-76 (lower panel, lane 4). Likewise, anti-NFATc1 failed to precipitate SLP-76 or RanGAP1 from resting or activated Jurkat cells (Figure S1B, lanes 3 and 4). Anti-SLP-76 coprecipitated RanGAP1, but no NFATc1 (lanes 5 and 6). These observations indicated that SLP-76 bound to RanGAP1, rather than RanBP2 or NFATc1.

Anti-SLP-76 coprecipitation of RanGAP1 was confirmed by MALDI-MS/MS (Figure S1C). Colloidal blue staining identified proteins that were coprecipitated by anti-SLP-76 (upper panel) that included GADs, ADAP-130 (*Fyb*-130) and 14-3-3. Six distinct peptides corresponding to RanGAP1 were detected (middle and lower boxes).

We also observed SLP-76 and the SLP-76/RanGAP complex in biochemically purified nuclear fractions (Figure 1F). Anti-CD3 ligation markedly increased SLP-76 in the nuclear envelope extract containing the NPC (left panel, lanes 5 and 6 versus lanes 1 and 2). $p56^{lck}$ was enriched in the cytosolic but not nuclear fraction (lower panel, lanes 4 and 8). Further, anti-SLP-76 coprecipitated RanGAP1 from the NPC extract of anti-CD3 ligated cells (right panel, lane 12). These data confirmed that anti-CD3 increased the presence of SUMO-RanGAP1 in the NPC.

SLP-76 Binding Promotes RanGAP1 Binding and Function at the NPC

We next mapped RanGAP1 binding to the N terminus of SLP-76 (Figure 2A). RanGAP1 was coexpressed with HA-tagged SLP-76 wild-type (WT) or mutants in SLP-76-deficient J14 T cells followed by anti-HA precipitation and anti-RanGAP1 blotting. Anti-CD3 ligation induced the complex formation as shown by anti-SLP-76 coprecipitation of SUMO-RanGAP1 (lane 2 versus lane 1). Random mutagenesis showed that mutation of lysine-56 to glutamic acid (termed K56E) disrupted the interaction (lanes 3 and 4), while mutation of residues 74/181/491 (i.e., 3KRE) had no effect (lanes 5 and 6). Blotting of lysates showed similar RanGAP1 expression in transfected cells (upper inset). HA-tagged SLP-76 WT and mutant expression was confirmed by anti-SLP-76 blotting (lower panel). Further, anti-CD3 ligation increased anti-SLP-76-associated RanGAP1 exchange activity by 7-fold, an effect lost with mutation of the K56 residue (Figure 2B). Blotting confirmed the concurrent loss of RanGAP1 binding with K56E (upper inset).

We also assessed whether SLP-76 and binding to RanGAP1 influenced RanGAP1 binding to the NPC. Anti-CD3 ligation increased SUMO-RanGAP1 coprecipitated by Mab414 (anti-NPC) over 2–15 min (Figure 2C, upper panel, lanes 3–7 versus lane 2). Nup62 coprecipitation served as a control (lower panel).

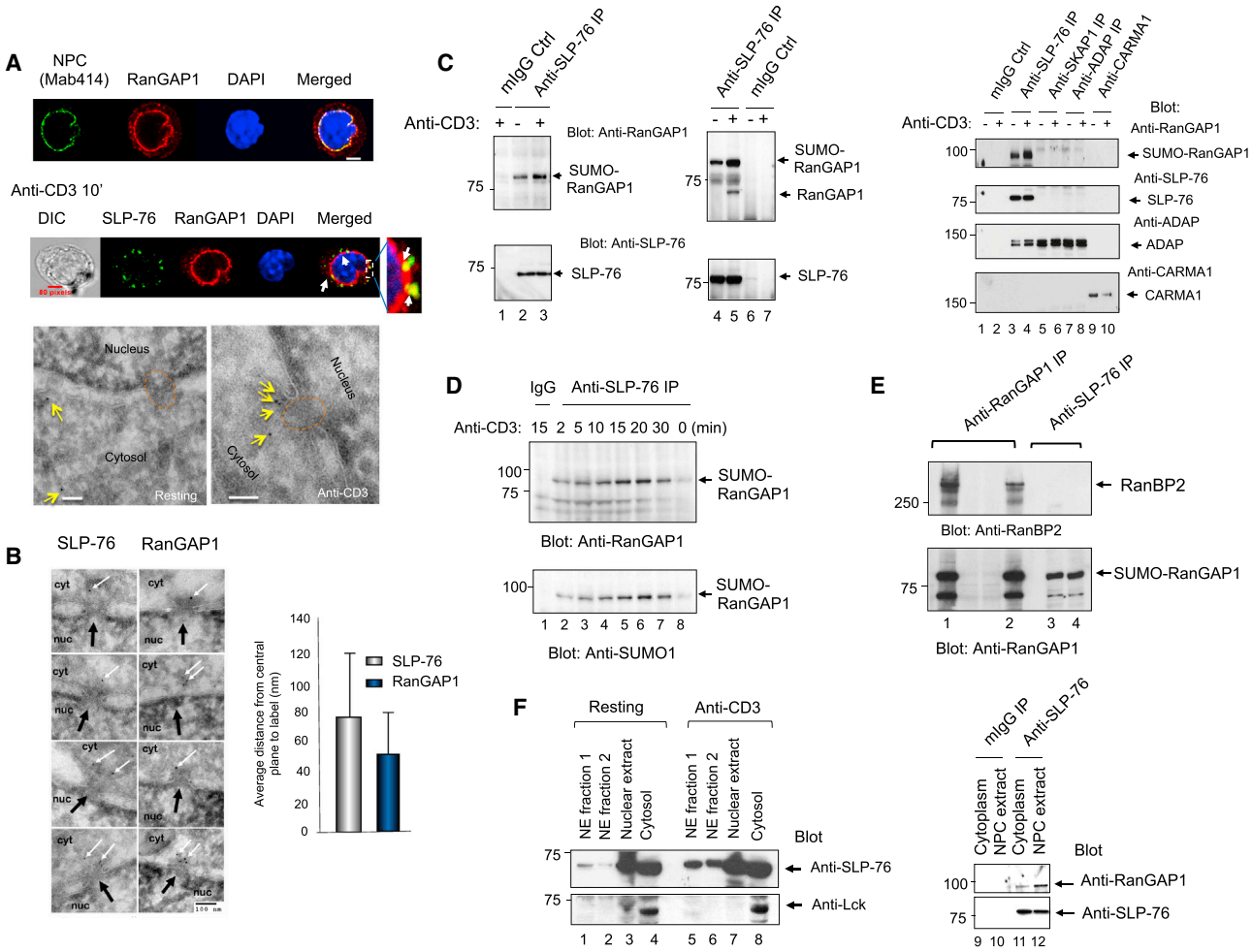

Figure 1. SLP-76 Localizes at the Cytoplasmic Face of the Nuclear Pore Complex and Interacts with SUMO-RanGAP1

(A) Confocal images of mouse DC27.10 T cells stained with Mab414-Alexa Fluor 488, anti-RanGAP1-Alexa Fluor 633, anti-SLP-76-Alexa Fluor 488 and DAPI (upper and middle panel) (scale bar, 5 μm). TEM images of gold-labeled anti-SLP-76 (yellow arrows) on the cytoplasmic face of the NPC (red dashed circle) (n = 3).

(B) TEM images of gold-labeled anti-SLP-76 and anti-RanGAP1 (white arrows) relative to the NPC (black arrows) upon anti-CD3 stimulation (left). Histogram shows distance of SLP-76 and RanGAP1 from central plane of NPC (right).

(C) Anti-SLP-76 coprecipitated RanGAP1. Resting or anti-CD3 activated DC27.10 T cells (left) or human peripheral blood lymphocytes (middle). Precipitation followed by blotting with anti-RanGAP1 (upper) or anti-SLP-76 (lower) (n = 4). (Right panel) RanGAP1 does not interact with immune adaptors SKAP1, ADAP, or CARMA1 (n = 3).

(D) Time course of RanGAP1 binding to SLP-76 upon anti-CD3 ligation. Blotted with anti-RanGAP1 (upper panel) or anti-SUMO1 (lower) (n = 3).

(E) Anti-SLP-76 does not coprecipitate RanBP2 from anti-CD3-stimulated Jurkat T cells. Blotted with anti-RanBP2 (upper panel) or anti-RanGAP1 (lower). Also see Figure S1.

(F) Anti-CD3 increases SLP-76 recruitment to the NPC. Mouse DC27.10 T cells stimulated with anti-CD3 followed by subcellular fractionation and blotted with anti-SLP-76 (left upper) or anti-lck (left lower). Anti-SLP-76 coprecipitates from NE fraction. Blotted with anti-RanGAP1 (right upper) and anti-SLP-76 (right lower) (n = 4).

The increase in coprecipitated SUMO-RanGAP1 from SLP-76-expressing cells at 15 min postligation (Figure 2D, lane 4 versus lane 3) was not evident in SLP-76-deficient J14 cells (lane 6 versus lane 5). Similarly, the anti-CD3-induced increase in SUMO-RanGAP1 in Mab414 precipitates from J14 cells expressing SLP-76 was not observed from cells with K56E (Figure 2E, lane 4 versus lane 3 and lane 6 versus lane 5; histogram). A time course also showed an increase in RanGAP1 that was not evident in K56E-expressing cells (Figure 2F, lanes 3 and 4 versus lane 2 and lanes 7 and 8 versus lane 6). SLP-76 expression and SLP-76-RanGAP1 binding is needed for the optimal anti-CD3-induced association of SUMO-RanGAP1 with the NPC.

We also observed that the specific activity for RanGAP1 for Ran-GTP was higher in anti-SLP-76 than anti-RanGAP1 precipitates lacking SLP-76 (Figure S2A, upper and lower panels). Specific activities were obtained by normalizing the activity relative to the amount of RanGAP1 in the precipitates as detected by blotting. Anti-RanGAP1 precipitates also showed lower

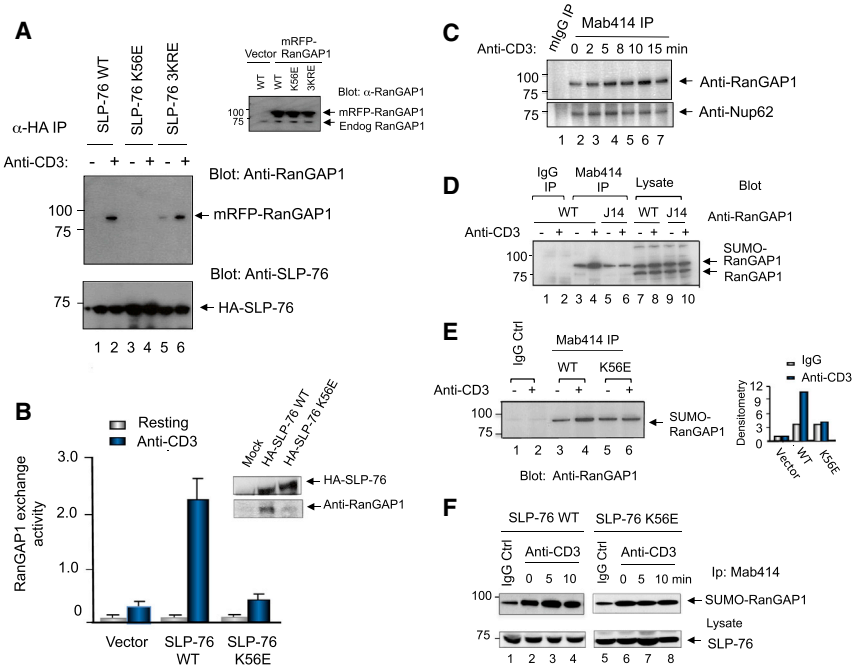

Figure 2. RanGAP1 Binds to SLP-76 Lysine 56 and Regulates RanGAP1 Binding to NPC

(A) RanGAP1 binds to lysine 56 in the SLP-76 N-terminal domain. SLP-76-deficient J14 T cells cotransfected with HA-tagged SLP-76 or mutants and mRFP-RanGAP1 (n = 3).

(B) Anti-CD3 increases RanGAP1 exchange activity that is lost with K56E. (Upper inset) Blot for HA-SLP-76 wild-type and K56E expression. Data are represented as mean ± SE of a representative experiment (n = 3). Also see Figure S2.

(C) Anti-CD3 ligation increases SUMO-RanGAP1 coprecipitated with anti-NPC Mab414. Cell lysates from DC27.10 T cells were stimulated with anti-CD3 for 15 min, followed by Mab414 precipitation and blotting with anti-RanGAP1 (upper) or Nup62 (lower) (n = 3).

(D) Anti-CD3-induced increase in SUMO-RanGAP1 association with the NPC is impaired in SLP-76-deficient T cells (n = 3).

(E) Anti-CD3-induced increase in SUMO-RanGAP1 association with the NPC is impaired in K56E-expressing cells. Right panel shows histogram of densitometric readings of SUMO-RanGAP1.

(F) Time course of anti-CD3-induced increase in SUMO-RanGAP1 coprecipitated by Mab414 from J14 cells expressing SLP-76 WT or K56E mutant. Anti-RanGAP1 blot (upper). Anti-SLP-76 blot of cell lysates (lower) (n = 4).

exchange activity from anti-CD3-activated cells expressing K56E compared to wild-type SLP-76 (Figure S2B). These observations suggested that, in addition to its role in promoting RanGAP1 binding to the NPC, SLP-76 binding to RanGAP1 increased its GAP activity for Ran-GTP.

SLP-76-RanGAP1 Binding Fails to Affect Proximal Signaling

It was next important to assess whether the mutation of K56 affected TCR proximal signaling (Figure 3). Microcluster formation is an early event needed for the stimulation of T cells (Bunnell et al., 2002; Yokosuka et al., 2005). SLP-76-EYFP and K56E-EYFP J14 cells were imaged on immobilized anti-CD3 on slides. Maximum overtime (MOT) images showed the formation and movement of clusters to central contact area (Figure 3Ai). No difference was detected between WT and K56E in terms of the number (ii), speed (iii), size (iv), or migration of clusters (v) (Movie S1). K56E and wild-type SLP-76 also bound to similar amounts of ADAP, GADS, and PLCγ1 (Figure 3B). In both cases, PLCγ1 shifted in migration in response to anti-CD3, consistent with increased phosphorylation. Anti-CD3-induced increase in intracellular calcium was also the same in J14 cells expressing K56E and WT SLP-76 (Figures 3C and S3A). The ionomycin-induced increase was also the same in SLP-76 WT and K56E-transfected cells (right panels).

NFATc1 dephosphorylation by calcineurin is a prerequisite for its nuclear translocation (Crabtree and Olson, 2002; Jain et al., 1992). J14 cells expressing K56E and WT SLP-76 showed a similar decrease in phosphorylated versus dephosphorylated NFAT in response to anti-CD3 ligation (Figure 3D). Further, a measurement of calcineurin phosphatase activity showed a similar increase in K56E and WT SLP-76-expressing cells (data not shown). These data indicated that K56E had no obvious effect on key aspects of proximal signaling by SLP-76.

SLP-76-RanGAP1 Binding Is Needed for Optimal NFATc1 and Rel/p65 Nuclear Entry

Despite having no effect on proximal signaling, the K56E mutant impaired NFATc1 entry into the nucleus. GFP-tagged NFATc1 nuclear translocation was imaged in J14 T cells expressing wild-type and K56E SLP-76 (Figure 4A). Transfected cells were incubated with anti-CD3 or isotype control (resting) for 5 min followed by anti-HA-Alexa Fluor 633 staining. Cells were scored positive when >70% of total GFP-NFATc1 overlapped with DAPI nuclear staining as quantified by ImageJ (Figure 4A, upper images; Figure S3B). Anti-HA staining was used as an internal control for WT or K56E HA-SLP-76 expression. While 45% of SLP-76-expressing cells showed nuclear NFATc1-GFP in response to anti-CD3, only 18% of cells expressing the K56E showed nuclear entry (Figure 4A, lower histogram). These data showed that SLP-76–RanGAP1 is needed for optimal anti-CD3-induced NFATc1 nuclear entry. K56E also impaired anti-CD3-induced transcription of an NFAT-driven IL-2 reporter construct by 50%–60% at different anti-CD3 concentrations (Figure 4B). Coexpression of SLP-76 and RanGAP1 also synergised to enhance anti-CD3-induced NFATc1 transcription, an effect impaired by K56E (Figure S4A). Anti-SLP-76 blotting confirmed similar transfected SLP-76 wild-type and K56E expression, comparable to endogenous SLP-76 in Jurkat cells (upper left inset). Anti-HA-blotting showed similar RanGAP1 expression in transfected cells including the higher MW SUMO-RanGAP1 (upper right panel). As a control, mRFP-RanGAP1 transfection showed

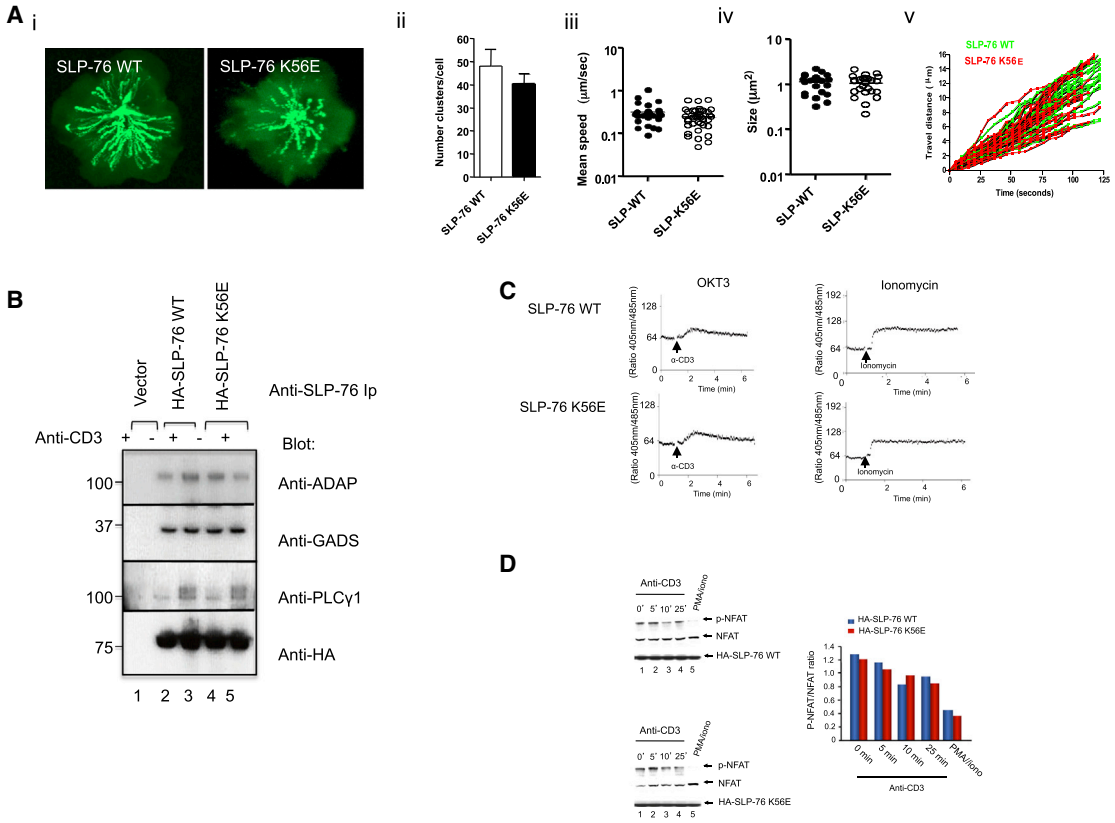

Figure 3. SLP-76 K56E Does Not Interfere with Early TCR Signaling Events

(A) K56E does not interfere with clustering. EYFP-SLP-76 WT and EYFP-SLP-76 K56E mutant cluster formation in Jurkat J14 cells on anti-CD3 coated coverslides (0–125 s). (i) Maximum overtime images; (ii) average number of microclusters; (iii) mean speed of EYFP-SLP-76 WT (black dots) and EYFP-SLP-76 K56E (white dots) clusters; (iv) size of microclusters; (v) trafficking analysis (n = 3).

(B) SLP-76 K56E associates normally with ADAP, GADS, and PLCγ1. J14 cells transfected with HA-SLP-76 WT or HA-SLP-76 K56E were stimulated by anti-CD3 followed by precipitation with anti-SLP-76 and blotting (n = 3).

(C) K56E supports calcium mobilization. Intracellular calcium levels were measured in J14 T cells transfected with HA-SLP-76 WT or HA-SLP-76 K56E mutant upon anti-CD3 stimulation (left) or ionomycin treatment (right) (n = 4). Also related to Figure S3A.

(D) SLP-76 WT- and SLP-76 K56E-expressing cells show the same levels of NFATc1 dephosphorylation. Transfected as above and stimulated with PMA/ionomycin, or anti-CD3 for various times followed by blotting with anti-NFAT1c1 (left) (n = 3). Histogram shows the similar decreasing phospho-NFATc1/NFATc1 ratio (right).

exclusive localization to the cytoplasm (Figure S4B). K56E expression also impaired NFAT transcription induced by ionomycin/phorbol ester (PMA), indicating that the SLP-76-RanGAP1 was needed for NFAT transcription induced by receptor-independent activation (Figure S4C). Intracellular staining for IL-2 also showed its reduced presence in SLP-76 K56E-expressing cells (Figure S4D).

SLP-76 K56E also inhibited the translocation of transport of NFκB p65/RelA into the nucleus (Figure 4C). GFP-RelA/p65 and HA-SLP-76 were cotransfected into J14 Jurkat cells, stimulated with anti-CD3, and imaged by confocal microscopy. SLP-76 K56E showed a reduction of 45% of GFP-RelA/p65 nuclear entry at 5 min and 65% at 15 min relative to WT SLP-76 (upper panels and lower histogram). Similar levels of GFP-RelA/p65 were expressed in cells with HA-SLP-76 WT and K56E (inset). Consistently, the anti-CD3-induced NF-κB driven luciferase reporter activity was 50%–60% lower in cells expressing K56E SLP-76 compared to WT SLP-76 (Figure 4D).

SLP-76-RanGAP1 Binding Is Needed for Optimal T Cell In Vivo Responses to Antigen

Given this, we next assessed whether the SLP-76-RanGAP1 interaction affected T cell responses in vivo (Figure 4E). DO11.10 transgenic T cells were transfected with either SLP-76-K56E or WT SLP-76, labeled with CFSE, and injected i.v. into Balb/c mice. Twenty-four hours later, 50 μg OVA peptide was then injected i.v. into mice (Greenwald et al., 2001). On day 6, spleens were extracted for FACs analysis (upper panel). Intracellular staining confirmed similar SLP-76 and K56E expression (middle panel). HA-SLP-76 was expressed similar to endogenous SLP-76 (inset). We found that while HA-SLP-76 WT supported OVA peptide-induced T cell proliferation, K56E-expressing cells were markedly impaired in their in vivo response to peptide (lower panel). These data confirmed that the SLP-76-RanGAP1 interaction plays a significant role in in vivo responses of T cells to antigen.

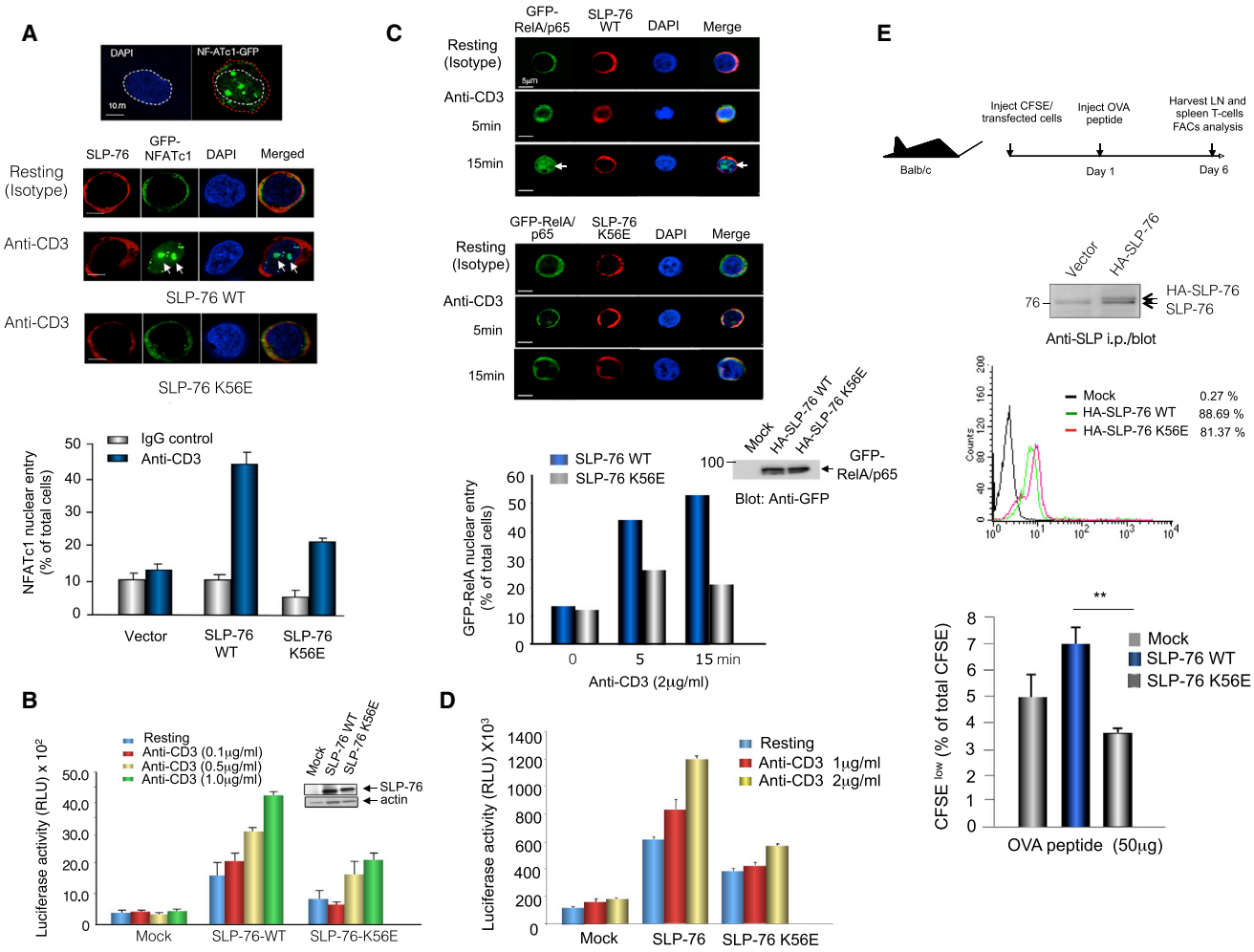

Figure 4. RanGAP1-SLP-76 Is Needed for Optimal NFATc1 and p65/RelA Nuclear Entry and In Vivo Responses to Antigen

(A) SLP-76 K56E shows impaired anti-CD3-induced-NFATc1 nuclear translocation. Images of cytoplasmic and nuclear GFP-NFATc in J14 T cells expressing HA-SLP-76 WT or HA-SLP-76 K56E. (Upper panel) Example of lines that delineate DAPI stained nucleus (white dotted line) from total cell (red dotted line). Also see Figure S3B. Histogram showing percentage of cells with nuclear NFATc1 (lower). Data are represented as a means of ± SD from a representative experiment (n = 3).

(B) SLP-76 K56E impairs anti-CD3-induced NFAT transcription activity. Anti-CD3 activation of Jurkat J14 cells with SLP-76 WT or SLP-76 K56E and NFAT (3x) luciferase reporter. (Inset) Expression levels of transfected SLP-76WT and mutant K56E. Data are means of ± SD from a representative experiment (n = 4).

(C) SLP-76 K56E impairs NFκB p65 (RelA) nuclear entry. Anti-CD3 stimulated J14 Jurkat cells expressing GFP-RelA/p65 and HA-SLP-76 or HA-K56E. Image of cells with SLP-76 (upper) or K56E (middle). Histogram showing percentage GFP-p65/RelA entry into nucleus (lower). (Upper inset) Blotting with anti-GFP show equal GFP-RelA/p65 in SLP-76 WT and K56E cells.

(D) Luciferase NF-kB reporter levels impaired in K56E-expressing J14 cells. Cells were transfected with SLP-76 or K56E plus a luciferase NF-kB reporter construct of interleukin 2 promoter. Data are means of ± SD from a representative experiment (n = 2). Also see Figure S4.

(E) RanGAP1-SLP-76 binding is needed for optimal in vivo responses of DO11.10 T cells to OVA peptide. CFSE-labeled DO11.10 CD4+ T cells were i.v. injected into the tail of Balb/c mice, followed by I.V. injection of 50 ug OVA- peptide 24 hr later. Experimental design (upper). Intracellular staining of transfected cells for SLP-76 wild-type and K56E (middle). (Inset) Anti-SLP-76 blotting of cell lysate showed that the level of expressed HA-SLP-76 is similar to endogenous SLP-76. Proliferation as measured by FACs analysis of CFSE intensity at day 6 (percentage CFSE low relative to total CFSE) (lower). Data are means of ± SD from representative experiments. Differences between means were tested using two-tailed unpaired Student's t test; *p < 0.05 was considered significant.

DISCUSSION

Although the NPC controls the entry of transcription factors into nucleus in response to antigen receptor ligation on T cells, it has been unclear whether cytoplasmic adaptors directly modulate the NPC. The cytoplasmic localization of NPC filaments makes them ideal targets. Our findings now identify immune cell adaptor SLP-76 binding to SUMO-RanGAP1 of the NPC as a mechanism to ensure the optimal transport of NFATc1 and RelA/p65 in the nucleus in response to antigen-receptor ligation. We found that this surprising interaction accounts for at least 40%–50% of NFATc1 and NF-κB p65 entry into nucleus of

T cells. The interaction represents a second checkpoint for NFATc1 nuclear entry, and may reflect the immense pressure on T cells to induce a rapid response to infection.

SLP-76 bound to RanGAP1, an event increased by TCR antigen receptor ligation. The principle form was SUMO-RanGAP1 that is exclusively associated with NPC filaments. SUMO1 is added to residue K526 of RanGAP1 and regulates the RanGDP-GTP gradient for importin α/β-dependent nuclear import (Mahajan et al., 1998). Specificity was shown by the failure of antibodies to ADAP, SKAP1, and CARMA1 to coprecipitate RanGAP1. SLP-76-SUMO-RanGAP1 was seen in mouse and human cell lines and primary cells, and appeared to occur maximally as a later event following TCR ligation. Its presence was confirmed by mass spectrometry after a late activation period, but is less evident in precipitates from T cells activated over shorter periods (Roncagalli et al., 2014). Remarkably, TEM showed that 76% of NPCs had at least one gold particle of SLP-76 with an average distance of 35 nm from the cytoplasmic face of the NPC, a distance comparable to RanGAP1. We found that binding depended on lysine 56 in SLP-76, where its mutation caused a loss of RanGAP1 binding and associated GTP/GDP exchange activity. Whether posttranslational modifications to K56 such as SUMOylation facilitate the interaction is unclear. Preliminary results with MaxQuant matching and Q-exactive failed to show SUMOylation (data not shown). SLP-76 therefore interfaces with the NPC complex by binding to SUMO-RanGAP1 of the cytoplasmic filaments of the pore complex.

Mechanistically, anti-CD3 ligation increased SLP-76 binding to RanGAP1 as well as GAP activity and complex binding to the NPC, in accord with the TEM studies. Antigen receptor modulation of RanGAP1 activity has not been previously reported. Further, SLP-76 affected RanGAP1 by acting on its binding to the NPC and GTP-GDP exchange activity. J14 cells lacking SLP-76, or transfected with K56E, had reduced coprecipitated RanGAP1 with MAb414, and lower RanGAP1 activity when normalized to levels of coprecipitated protein. It was the anti-CD3 stimulated increase (rather than basal activity) that was affected by SLP-76 deficiency, or the K56E mutant. The enhanced presence and activity of RanGAP1 at the NPC are in keeping with its role in regulating the Ran-GDP/GTP gradient (Quimby and Dasso, 2003).

Importantly, we showed that the SLP-76-RanGAP1 regulated the nuclear entry of two key transcription factors, NFATc1 and NF-κB p65. K56E impaired entry of each to the same degree. Further, SLP-76 and RanGAP1 synergized to greatly enhance anti-CD3-induced NFAT-driven transcription, an effect lost with the K56E mutant. Importantly, K56E had no effect on proximal signaling events such as SLP-76 microcluster formation, calcium mobilization, or NFATc1 dephosphorylation. Despite this, the K56E mutant impaired NFATc1-GFP and GFP-RelA/p65 nuclear entry and transcription by 40%–50%. An even more pronounced effect was observed in the in vivo responses of DO11.10 T cells to OVA peptide. NFAT entry therefore involves two steps, canonical dephosphorylation followed by direct SLP-76 binding to RanGAP1 and regulation at the NPC. This second tier of regulation may reflect the need for rapid transcription to respond to infections by viruses and other pathogens. The full range of cargo and the different receptors (i.e., innate versus adaptive) involved in the pathway remains to be determined. However, a broad effect on signaling was suggested by K56E inhibition of receptor-independent stimulation by PMA/ionomycin.

The SLP-76-SUMO-RanGAP1 interaction is unique to immune cells and has evolved to complement generic NPC regulation by RanBP2 that helps to localize SUMO1-RanGAP1 and UBC9 at the NPC. SLP-76 bound to RanGAP1, but not RanBP2, suggesting that SLP-76 is likely to complement RanBP2. Further, K56E preferentially affected the TCR/CD3 increase in the RanGAP1-NPC association in accord with a specific connection to TCR signaling. Whether SLP-76 homologs with a similar function exist in other cell types such as neuron cells remains to be determined.

Whether SLP-76 is derived from the cell surface or a distinct pool is unclear. SLP-76 microclusters accumulate in a perinuclear structure (Bunnell et al., 2002). It is also a later event, peaking at 15–20 min postligation, consistent with time needed to move from the cell surface to the nucleus. We postulate that SLP-76 surface clusters may eventually migrate and regulate the NPC. Alternatively, a separate pool of compartmentalised SLP-76 could also interact. Future studies will determine the range of cargo regulated by the SLP-76-RanGAP1 complex and whether it is needed for nuclear entry induced by other receptors such as Toll-like receptors (TLRs).

EXPERIMENTAL PROCEDURES

Cell Culture and Reagents

Jurkat, SLP-76-deficient J14, T8.1, and DC27.10 cells were cultured as previously described (Liu et al., 2010; Raab et al., 1999; Schneider et al., 2008). Antibodies included anti-human CD3 (OKT3), hamster anti-mouse CD3 145-2C11 (ATCC), anti-SLP-76 (BioXcell, West Lebanon, NH), anti-RanGAP1 (Santa Cruz Biotechnology, USA), Mab414 (Covance), anti-SUMO1 (gift from R. Hay, Dundee, UK), anti-Carma1 (Cell Signaling USA), anti-HA (Covance), anti-Lck, anti-ADAP, anti-SKAP1, and anti-GADS (Upstate Biotechnology, USA), anti-NF-ATc1 (Santa Cruz Biotechnology, Santa Cruz, CA, USA), anti-RanBP2 (Thermo Scientific), and anti-actin (Sigma-Aldrich, USA). Carboxyfluorescein diacetate succinimidyl ester (CFSE) was purchased from Sigma (Poole, UK). HA-tagged SLP-76 and RanGAP1, SLP-76-YFP, and the K56E SLP-76 mutant were constructed as described in the Supplemental Experimental Procedures.

Transfection and Stimulation

Mouse and human T cells were stimulated with 2–5 μg/ml of 145-2C11 or OKT3 as described (Raab et al., 1999). Jurkat and J14 T cells were transfected by microporation (Digital Bio Technology) using a single pulse of 30 ms at 1410 V, while DC27.10 cells received 2 pulses of 20 ms at 1,400 V. Human primary T cells were transfected using a single pulse of 20 ms at 2,259 V. Primary naive mouse cells were transfected with various vectors using the Amaxa Nucleofector Kit (Lonza, Germany).

RanGAP1 GAP Activity Assays

RanGAP1 activity was quantified using either a Phos-Free Phosphate Assay Kit (Cytoskeleton Inc., Denver, CO) or a radioactive assay as described in Bischoff et al. (1994) and in the Supplemental Experimental Procedures. RanGAP1 GAP activity measured by isotope labeling (Figures 2B and S2A), or using a nonradioactive protocol (Figure S2B), $^{**}p < 0.01$, $^{***}p < 0.001$ versus SLP-76 WT. The average results were shown from three independent experiments.

Immune Precipitation and Nuclear Pore Fraction

Precipitation and blotting were performed as described (Raab et al., 2011). Nuclear pore fractions were separated from cytoplasmic fractions of DC27.10

T cells by using the Thermo NE-PER Nuclear and Cytoplasmic Extraction Kit (Fischer Scientific).

Liquid Chromatography Tandem Mass Spectrometry (LC-MS/MS)

Bands from anti-SLP-76 precipitation from DC27.10 or T8.1 T cells were analyzed by liquid chromatography-tandem mass spectrometry (LC-MS/MS) (conducted by Cambridge Centre for Proteomics, Cambridge University) as described in the Supplemental Experimental Procedures. Database searches of the mass fingerprint data were performed using Mascot (http://www.matrixscience.com). For tandem ms/ms analysis, desalted peptides were delivered to a ThermoFinnigan LCQ Classic ion-trap mass spectrometer using a static nanospray needle (Thermo Proxeon). Fragment ions were matched to possible sequence interpretations using MS-Product and/or MS-Tag (http://prospector.ucsf.edu/).

Immunofluorescence and Confocal Imaging

Immunofluorescence and confocal imaging were conducted as previously described (Liu et al., 2010; Purbhoo et al., 2010) and as described in the Supplemental Experimental Procedures. J14 cells were cotransfected with GFP-NFATc1 or GFP-RelA/p65 together with either HA-SLP-76 WT or HA-SLP76 K56E.

In Vivo Adoptive T Cell Transfer Assay

Adoptive T cell transfer assay were conducted as described in the Supplemental Experimental Procedures. DO11.10 T cells were transfected with HA-SLP-76 or HA-SLP-76 K53E and labeled with CFSE (5 μM). Proliferation of CFSE labeled T cells was assessed 6 days after the OVA-peptide injections by FACs analysis.

Transmission Electron Microscopy

TEM was conducted as described (Zuleger et al., 2011). Images were taken on a Hitachi H7600 electron microscope. In order to measure the distances, since the cytoplasmic ring could not be directly visualized, first the distance from the central plane to the particle was measured, then the known distance (40 nm) from the central plane to the top of the cytoplasmic ring (Maimon et al., 2012) was subtracted to give the ring-label distance.

Measurement of Intracellular Calcium

SLP-76-deficient J14 cells transfected with pcDNA-SLP-76 WT or K56E mutant were subjected to calcium influx measurement with Indo-1 (Invitrogen) (Parry et al., 2000). For statistical comparisons, the calcium response was normalized and expressed as the ratio of the maximum peak poststimulation to baseline. Kinetic plots were generated on ligated (Indo-1-labeled) cells using FlowJo software.

Promoter Reporter Assays

Promoter Reporter Assays were conducted as previously described (Liu et al., 2010; Raab et al., 1999; Veale et al., 1999) and as described in the Supplemental Experimental Procedures. Luciferase activity was measured using a luminometer (MicroLumat, EG&G Berthold).

SUPPLEMENTAL INFORMATION

Supplemental Information includes four figures, one movie, and Supplemental Experimental Procedures and can be found with this article at http://dx.doi.org/10.1016/j.molcel.2015.07.015.

AUTHOR CONTRIBUTIONS

C.E.R. conceived of the original basis of the project and coordinated the activities of coauthors; H.L. and H.S. carried out the biochemical, cellular and imaging studies; A.R. carried out GAP assays and imaging studies; H.L., C.R., and M.W.G. conducted the transmission electron microscopy; C.E.R and H.L. wrote the manuscript with contributions from H.S., A.R., C.R., and M.W.G.

ACKNOWLEDGMENTS

The work was supported by the program grant from Wellcome Trust 092627/Z/10/Z (C.E.R.).

Received: October 23, 2014
Revised: June 1, 2015
Accepted: July 17, 2015
Published: August 27, 2015

REFERENCES

Allen, T.D., Rutherford, S.A., Murray, S., Drummond, S.P., Goldberg, M.W., and Kiseleva, E. (2008). Scanning electron microscopy of nuclear structure. Methods Cell Biol. *88*, 389–409.

Bernier-Villamor, V., Sampson, D.A., Matunis, M.J., and Lima, C.D. (2002). Structural basis for E2-mediated SUMO conjugation revealed by a complex between ubiquitin-conjugating enzyme Ubc9 and RanGAP1. Cell *108*, 345–356.

Bischoff, F.R., Klebe, C., Kretschmer, J., Wittinghofer, A., and Ponstingl, H. (1994). RanGAP1 induces GTPase activity of nuclear Ras-related Ran. Proc. Natl. Acad. Sci. USA *91*, 2587–2591.

Bubeck Wardenburg, J., Fu, C., Jackman, J.K., Flotow, H., Wilkinson, S.E., Williams, D.H., Johnson, R., Kong, G., Chan, A.C., and Findell, P.R. (1996). Phosphorylation of SLP-76 by the ZAP-70 protein-tyrosine kinase is required for T-cell receptor function. J. Biol. Chem. *271*, 19641–19644.

Bubeck Wardenburg, J., Pappu, R., Bu, J.Y., Mayer, B., Chernoff, J., Straus, D., and Chan, A.C. (1998). Regulation of PAK activation and the T cell cytoskeleton by the linker protein SLP-76. Immunity *9*, 607–616.

Bunnell, S.C., Diehn, M., Yaffe, M.B., Findell, P.R., Cantley, L.C., and Berg, L.J. (2000). Biochemical interactions integrating Itk with the T cell receptor-initiated signaling cascade. J. Biol. Chem. *275*, 2219–2230.

Bunnell, S.C., Hong, D.I., Kardon, J.R., Yamazaki, T., McGlade, C.J., Barr, V.A., and Samelson, L.E. (2002). T cell receptor ligation induces the formation of dynamically regulated signaling assemblies. J. Cell Biol. *158*, 1263–1275.

Chatel, G., and Fahrenkrog, B. (2012). Dynamics and diverse functions of nuclear pore complex proteins. Nucleus *3*, 162–171.

Crabtree, G.R., and Olson, E.N. (2002). NFAT signaling: choreographing the social lives of cells. Cell *109* (*Suppl*), S67–S79.

D'Angelo, M.A., and Hetzer, M.W. (2008). Structure, dynamics and function of nuclear pore complexes. Trends Cell Biol. *18*, 456–466.

da Silva, A.J., Li, Z., de Vera, C., Canto, E., Findell, P., and Rudd, C.E. (1997). Cloning of a novel T-cell protein FYB that binds FYN and SH2-domain-containing leukocyte protein 76 and modulates interleukin 2 production. Proc. Natl. Acad. Sci. USA *94*, 7493–7498.

Di Bartolo, V., Montagne, B., Salek, M., Jungwirth, B., Carrette, F., Fourtane, J., Sol-Foulon, N., Michel, F., Schwartz, O., Lehmann, W.D., and Acuto, O. (2007). A novel pathway down-modulating T cell activation involves HPK-1-dependent recruitment of 14-3-3 proteins on SLP-76. J. Exp. Med. *204*, 681–691.

Ghosh, S., and Karin, M. (2002). Missing pieces in the NF-kappaB puzzle. Cell *109* (*Suppl*), S81–S96.

Grasis, J.A., Guimond, D.M., Cam, N.R., Herman, K., Magotti, P., Lambris, J.D., and Tsoukas, C.D. (2010). In vivo significance of ITK-SLP-76 interaction in cytokine production. Mol. Cell. Biol. *30*, 3596–3609.

Greenwald, R.J., Boussiotis, V.A., Lorsbach, R.B., Abbas, A.K., and Sharpe, A.H. (2001). CTLA-4 regulates induction of anergy in vivo. Immunity *14*, 145–155.

Hoelz, A., Debler, E.W., and Blobel, G. (2011). The structure of the nuclear pore complex. Annu. Rev. Biochem. *80*, 613–643.

Hutten, S., Flotho, A., Melchior, F., and Kehlenbach, R.H. (2008). The Nup358-RanGAP complex is required for efficient importin alpha/beta-dependent nuclear import. Mol. Biol. Cell *19*, 2300–2310.

Jackman, J.K., Motto, D.G., Sun, Q., Tanemoto, M., Turck, C.W., Peltz, G.A., Koretzky, G.A., and Findell, P.R. (1995). Molecular cloning of SLP-76, a 76-kDa tyrosine phosphoprotein associated with Grb2 in T cells. J. Biol. Chem. *270*, 7029–7032.

Jain, J., McCaffrey, P.G., Valge-Archer, V.E., and Rao, A. (1992). Nuclear factor of activated T cells contains Fos and Jun. Nature *356*, 801–804.

Jordan, M.S., Singer, A.L., and Koretzky, G.A. (2003). Adaptors as central mediators of signal transduction in immune cells. Nat. Immunol. *4*, 110–116.

Lee, G.W., Melchior, F., Matunis, M.J., Mahajan, R., Tian, Q., and Anderson, P. (1998). Modification of Ran GTPase-activating protein by the small ubiquitin-related modifier SUMO-1 requires Ubc9, an E2-type ubiquitin-conjugating enzyme homologue. J. Biol. Chem. *273*, 6503–6507.

Liu, J., Kang, H., Raab, M., da Silva, A.J., Kraeft, S.K., and Rudd, C.E. (1998). FYB (FYN binding protein) serves as a binding partner for lymphoid protein and FYN kinase substrate SKAP55 and a SKAP55-related protein in T cells. Proc. Natl. Acad. Sci. USA *95*, 8779–8784.

Liu, H., Purbhoo, M.A., Davis, D.M., and Rudd, C.E. (2010). SH2 domain containing leukocyte phosphoprotein of 76-kDa (SLP-76) feedback regulation of ZAP-70 microclustering. Proc. Natl. Acad. Sci. USA *107*, 10166–10171.

Mahajan, R., Delphin, C., Guan, T., Gerace, L., and Melchior, F. (1997). A small ubiquitin-related polypeptide involved in targeting RanGAP1 to nuclear pore complex protein RanBP2. Cell *88*, 97–107.

Mahajan, R., Gerace, L., and Melchior, F. (1998). Molecular characterization of the SUMO-1 modification of RanGAP1 and its role in nuclear envelope association. J. Cell Biol. *140*, 259–270.

Maimon, T., Elad, N., Dahan, I., and Medalia, O. (2012). The human nuclear pore complex as revealed by cryo-electron tomography. Structure *20*, 998–1006.

Marinari, B., Costanzo, A., Viola, A., Michel, F., Mangino, G., Acuto, O., Levrero, M., Piccolella, E., and Tuosto, L. (2002). Vav cooperates with CD28 to induce NF-kappaB activation via a pathway involving Rac-1 and mitogen-activated kinase kinase 1. Eur. J. Immunol. *32*, 447–456.

Matunis, M.J., Coutavas, E., and Blobel, G. (1996). A novel ubiquitin-like modification modulates the partitioning of the Ran-GTPase-activating protein RanGAP1 between the cytosol and the nuclear pore complex. J. Cell Biol. *135*, 1457–1470.

Melchior, F., Guan, T., Yokoyama, N., Nishimoto, T., and Gerace, L. (1995). GTP hydrolysis by Ran occurs at the nuclear pore complex in an early step of protein import. J. Cell Biol. *131*, 571–581.

Müller, M.R., and Rao, A. (2010). NFAT, immunity and cancer: a transcription factor comes of age. Nat. Rev. Immunol. *10*, 645–656.

Musci, M.A., Hendricks-Taylor, L.R., Motto, D.G., Paskind, M., Kamens, J., Turck, C.W., and Koretzky, G.A. (1997). Molecular cloning of SLAP-130, an SLP-76-associated substrate of the T cell antigen receptor-stimulated protein tyrosine kinases. J. Biol. Chem. *272*, 11674–11677.

Parry, C.M., Simas, J.P., Smith, V.P., Stewart, C.A., Minson, A.C., Efstathiou, S., and Alcami, A. (2000). A broad spectrum secreted chemokine binding protein encoded by a herpesvirus. J. Exp. Med. *191*, 573–578.

Pichler, A., Gast, A., Seeler, J.S., Dejean, A., and Melchior, F. (2002). The nucleoporin RanBP2 has SUMO1 E3 ligase activity. Cell *108*, 109–120.

Pivniouk, V., Tsitsikov, E., Swinton, P., Rathbun, G., Alt, F.W., and Geha, R.S. (1998). Impaired viability and profound block in thymocyte development in mice lacking the adaptor protein SLP-76. Cell *94*, 229–238.

Purbhoo, M.A., Liu, H., Oddos, S., Owen, D.M., Neil, M.A., Pageon, S.V., French, P.M., Rudd, C.E., and Davis, D.M. (2010). Dynamics of subsynaptic vesicles and surface microclusters at the immunological synapse. Sci. Signal. *3*, ra36.

Quimby, B.B., and Dasso, M. (2003). The small GTPase Ran: interpreting the signs. Curr. Opin. Cell Biol. *15*, 338–344.

Raab, M., da Silva, A.J., Findell, P.R., and Rudd, C.E. (1997). Regulation of Vav-SLP-76 binding by ZAP-70 and its relevance to TCR zeta/CD3 induction of interleukin-2. Immunity *6*, 155–164.

Raab, M., Kang, H., da Silva, A., Zhu, X., and Rudd, C.E. (1999). FYN-T-FYB-SLP-76 interactions define a T-cell receptor zeta/CD3-mediated tyrosine phosphorylation pathway that up-regulates interleukin 2 transcription in T-cells. J. Biol. Chem. *274*, 21170–21179.

Raab, M., Wang, H., Lu, Y., Smith, X., Wu, Z., Strebhardt, K., Ladbury, J.E., and Rudd, C.E. (2010). T cell receptor "inside-out" pathway via signaling module SKAP1-RapL regulates T cell motility and interactions in lymph nodes. Immunity *32*, 541–556.

Raab, M., Smith, X., Matthes, Y., Strebhardt, K., and Rudd, C.E. (2011). SKAP1 PH domain determines RAPL membrane localization and Rap1 complex formation for TCR activation of LFA-1. J. Biol. Chem. *286*, 29663–29670.

Roncagalli, R., Hauri, S., Fiore, F., Liang, Y., Chen, Z., Sansoni, A., Kanduri, K., Joly, R., Malzac, A., Lähdesmäki, H., et al. (2014). Quantitative proteomics analysis of signalosome dynamics in primary T cells identifies the surface receptor CD6 as a Lat adaptor-independent TCR signaling hub. Nat. Immunol. *15*, 384–392.

Rudd, C.E. (1999). Adaptors and molecular scaffolds in immune cell signaling. Cell *96*, 5–8.

Rudd, C.E., Trevillyan, J.M., Dasgupta, J.D., Wong, L.L., and Schlossman, S.F. (2010). Pillars article: the CD4 receptor is complexed in detergent lysates to a protein-tyrosine kinase (pp58) from human T lymphocytes. 1988. J. Immunol. *185*, 2645–2649.

Samelson, L.E. (2002). Signal transduction mediated by the T cell antigen receptor: the role of adapter proteins. Annu. Rev. Immunol. *20*, 371–394.

Schneider, H., Guerette, B., Guntermann, C., and Rudd, C.E. (2000). Resting lymphocyte kinase (Rlk/Txk) targets lymphoid adaptor SLP-76 in the cooperative activation of interleukin-2 transcription in T-cells. J. Biol. Chem. *275*, 3835–3840.

Schneider, H., Smith, X., Liu, H., Bismuth, G., and Rudd, C.E. (2008). CTLA-4 disrupts ZAP70 microcluster formation with reduced T cell/APC dwell times and calcium mobilization. Eur. J. Immunol. *38*, 40–47.

Sen, R. (2011). The origins of NF-κB. Nat. Immunol. *12*, 686–688.

Shibasaki, F., Price, E.R., Milan, D., and McKeon, F. (1996). Role of kinases and the phosphatase calcineurin in the nuclear shuttling of transcription factor NF-AT4. Nature *382*, 370–373.

Shui, J.W., Boomer, J.S., Han, J., Xu, J., Dement, G.A., Zhou, G., and Tan, T.H. (2007). Hematopoietic progenitor kinase 1 negatively regulates T cell receptor signaling and T cell-mediated immune responses. Nat. Immunol. *8*, 84–91.

Smith-Garvin, J.E., Koretzky, G.A., and Jordan, M.S. (2009). T cell activation. Annu. Rev. Immunol. *27*, 591–619.

Thaker, Y.R., Schneider, H., and Rudd, C.E. (2015). TCR and CD28 activate the transcription factor NF-κB in T-cells via distinct adaptor signaling complexes. Immunol. Lett. *163*, 113–119.

Veale, M., Raab, M., Li, Z., da Silva, A.J., Kraeft, S.K., Weremowicz, S., Morton, C.C., and Rudd, C.E. (1999). Novel isoform of lymphoid adaptor FYN-T-binding protein (FYB-130) interacts with SLP-76 and up-regulates interleukin 2 production. J. Biol. Chem. *274*, 28427–28435.

Wang, H., and Rudd, C.E. (2008). SKAP-55, SKAP-55-related and ADAP adaptors modulate integrin-mediated immune-cell adhesion. Trends Cell Biol. *18*, 486–493.

Werner, A., Flotho, A., and Melchior, F. (2012). The RanBP2/RanGAP1*SUMO1/Ubc9 complex is a multisubunit SUMO E3 ligase. Mol. Cell *46*, 287–298.

Williamson, D.J., Owen, D.M., Rossy, J., Magenau, A., Wehrmann, M., Gooding, J.J., and Gaus, K. (2011). Pre-existing clusters of the adaptor Lat do not participate in early T cell signaling events. Nat. Immunol. *12*, 655–662.

Wu, J., Motto, D.G., Koretzky, G.A., and Weiss, A. (1996). Vav and SLP-76 interact and functionally cooperate in IL-2 gene activation. Immunity *4*, 593–602.

Wu, H., Peisley, A., Graef, I.A., and Crabtree, G.R. (2007). NFAT signaling and the invention of vertebrates. Trends Cell Biol. *17*, 251–260.

Yablonski, D., Kuhne, M.R., Kadlecek, T., and Weiss, A. (1998). Uncoupling of nonreceptor tyrosine kinases from PLC-gamma1 in an SLP-76-deficient T cell. Science *281*, 413–416.

Yablonski, D., Kadlecek, T., and Weiss, A. (2001). Identification of a phospholipase C-gamma1 (PLC-gamma1) SH3 domain-binding site in SLP-76 required for T-cell receptor-mediated activation of PLC-gamma1 and NFAT. Mol. Cell. Biol. *21*, 4208–4218.

Yokosuka, T., Sakata-Sogawa, K., Kobayashi, W., Hiroshima, M., Hashimoto-Tane, A., Tokunaga, M., Dustin, M.L., and Saito, T. (2005). Newly generated T cell receptor microclusters initiate and sustain T cell activation by recruitment of Zap70 and SLP-76. Nat. Immunol. *6*, 1253–1262.

Zhang, W., Sloan-Lancaster, J., Kitchen, J., Trible, R.P., and Samelson, L.E. (1998). LAT: the ZAP-70 tyrosine kinase substrate that links T cell receptor to cellular activation. Cell *92*, 83–92.

Zuleger, N., Kelly, D.A., Richardson, A.C., Kerr, A.R., Goldberg, M.W., Goryachev, A.B., and Schirmer, E.C. (2011). System analysis shows distinct mechanisms and common principles of nuclear envelope protein dynamics. J. Cell Biol. *193*, 109–123.

Molecular Cell, Volume *59*

Supplemental Information

The Immune Adaptor SLP-76 Binds to SUMO-RANGAP1 at Nuclear Pore Complex Filaments to Regulate Nuclear Import of Transcription Factors in T Cells

Hebin Liu, Helga Schneider, Asha Recino, Christine Richardson, Martin W. Goldberg, and Christopher E. Rudd

Figure S1

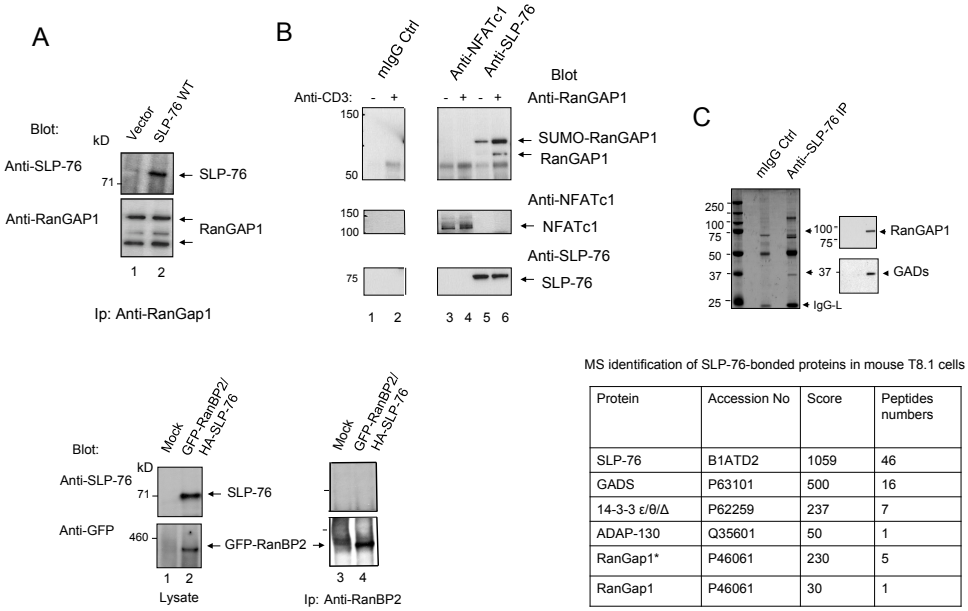

MS identification of SLP-76-bonded proteins in mouse T8.1 cells

Protein	Accession No	Score	Peptides numbers
SLP-76	B1ATD2	1059	46
GADS	P63101	500	16
14-3-3 ε/θ/Δ	P62259	237	7
ADAP-130	Q35601	50	1
RanGap1*	P46061	230	5
RanGap1	P46061	30	1

(C) (continued)

tr|Q6NZB5|Q6NZB5_MOUSE **Mass:** 64005 **Score:** 230 **Matches:** 5(4) **Sequences:** 5(4) **emPAI:** 0.28
Rangap1 protein OS=Mus musculus GN=Rangap1
Check to include this hit in error tolerant search or archive report

Query	Observed	Mr(expt)	Mr(calc)	ppm	Miss	Score	Expect	Rank	Unique	Peptide
566	496.7580	991.5014	991.5008	0.63	0	33	0.012	1	U	K.GGVAMAETLK.T + Oxidation (M)
1076	568.3101	1134.6057	1134.6033	2.08	0	24	0.12	1	U	K.TQVAGGQLSFK.G
1593	638.8448	1275.6751	1275.6744	0.57	0	58	4.7e-05	1	U	K.TAVLDAIDALMK.K + Oxidation (M)
1902	704.3607	1406.7069	1406.7041	1.95	0	44	0.00094	1	U	R.VINLNDNTFTEK.G
2224	879.9641	1757.9135	1757.9047	5.02	0	71	2.2e-06	1	U	K.VSVLIVQQTDTSDPEK.V

Proteins matching the same set of peptides:
sp|P46061|RAGP1_MOUSE **Mass:** 64090 **Score:** 230 **Matches:** 5(4) **Sequences:** 5(4)
Ran GTPase-activating protein 1 OS=Mus musculus GN=Rangap1

Sumoylated RanGap1 identified from gel slice with MW range from 80-100 kD

tr|Q6NZB5|Q6NZB5_MOUSE **Mass:** 64005 **Score:** 30 **Matches:** 1(1) **Sequences:** 1(1) **emPAI:** 0.05
Rangap1 protein OS=Mus musculus GN=Rangap1
Check to include this hit in error tolerant search or archive report

Query	Observed	Mr(expt)	Mr(calc)	ppm	Miss	Score	Expect	Rank	Unique	Peptide
1231	704.3654	1406.7162	1406.7041	8.55	0	30	0.028	1	U	R.VINLNDNTFTEK.G

Proteins matching the same set of peptides:
tr|E9Q2J7|E9Q2J7_MOUSE **Mass:** 43303 **Score:** 30 **Matches:** 1(1) **Sequences:** 1(1)
Uncharacterized protein OS=Mus musculus GN=Rangap1
sp|P46061|RAGP1_MOUSE **Mass:** 64090 **Score:** 30 **Matches:** 1(1) **Sequences:** 1(1)
Ran GTPase-activating protein 1 OS=Mus musculus GN=Rangap1

Figure S2

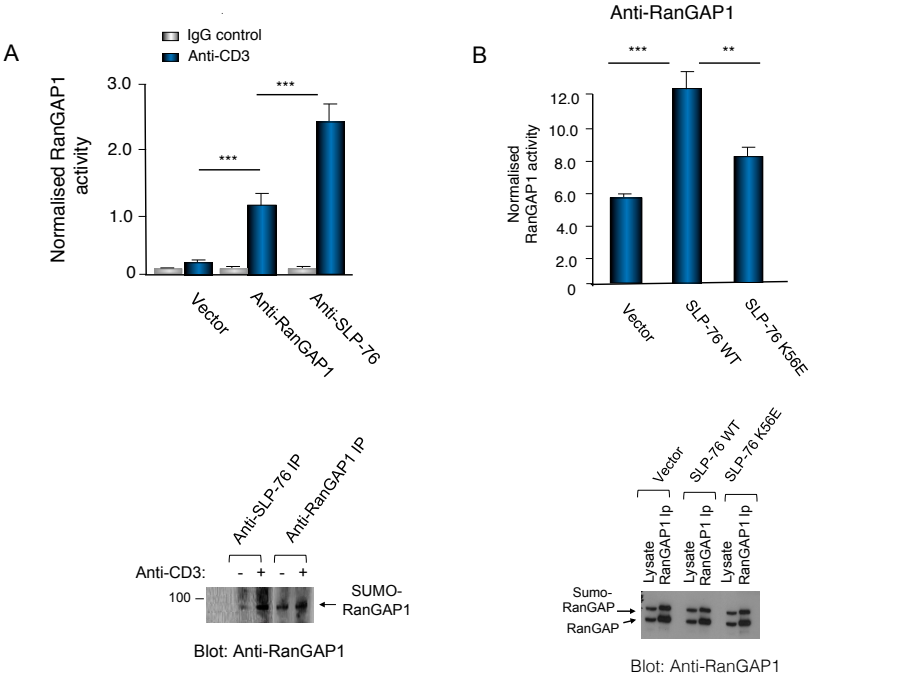
A
IgG control
Anti-CD3
Normalised RanGAP1 activity
3.0
2.0
1.0
0
***
***
Vector
Anti-RanGAP1
Anti-SLP-76
Anti-SLP-76 IP
Anti-RanGAP1 IP
Anti-CD3:
- + - +
100
SUMO-RanGAP1
Blot: Anti-RanGAP1
B
Anti-RanGAP1
***
**
Normalised RanGAP1 activity
12.0
10.0
8.0
6.0
4.0
2.0
0
Vector
SLP-76 WT
SLP-76 K56E
Vector
SLP-76 WT
SLP-76 K56E
Lysate
RanGAP1 Ip
Lysate
RanGAP1 Ip
Lysate
RanGAP1 Ip
Sumo-RanGAP
RanGAP
Blot: Anti-RanGAP1

Figure S3

A

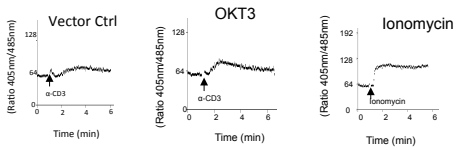
Vector Ctrl
OKT3
Ionomycin
(Ratio 405nm/485nm)
Time (min)
α-CD3
Ionomycin

B

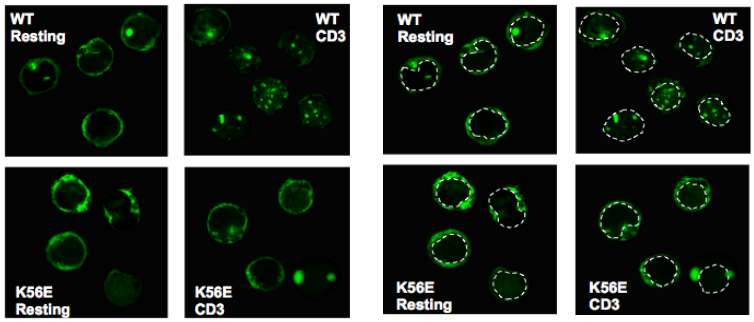
WT
Resting
WT
CD3
K56E
Resting
K56E
CD3

Figure S4

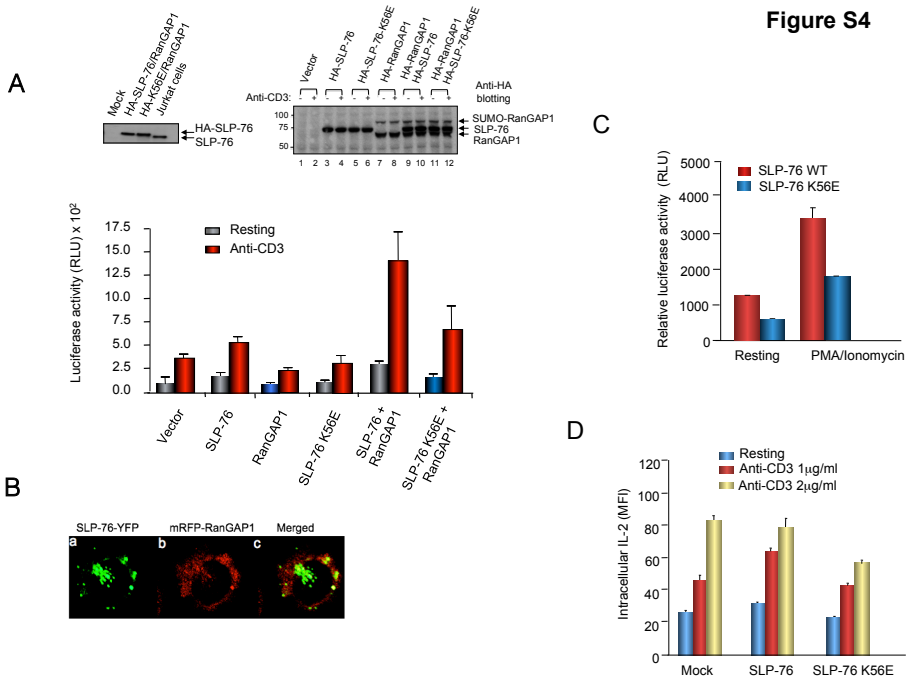
A
Mock
HA-SLP-76/RanGAP1
HA-K56E/RanGAP1
Jurkat cells
HA-SLP-76
SLP-76
Anti-CD3:
Vector
HA-SLP-76
HA-SLP-76-K56E
HA-RanGAP1
HA-RanGAP1 HA-SLP-76
HA-RanGAP1 HA-SLP-76-K56E
Anti-HA blotting
100
75
50
SUMO-RanGAP1
SLP-76
RanGAP1
1 2 3 4 5 6 7 8 9 10 11 12
Luciferase activity (RLU) x 10²
17.5
15.0
12.5
10.0
7.5
5.0
2.5
0.0
Resting
Anti-CD3
Vector
SLP-76
RanGAP1
SLP-76 K56E
SLP-76 + RanGAP1
SLP-76 K56E + RanGAP1
B
SLP-76-YFP
mRFP-RanGAP1
Merged
a
b
c
C
Relative luciferase activity (RLU)
5000
4000
3000
2000
1000
0
SLP-76 WT
SLP-76 K56E
Resting
PMA/Ionomycin
D
Intracellular IL-2 (MFI)
120
100
80
60
40
20
0
Resting
Anti-CD3 1μg/ml
Anti-CD3 2μg/ml
Mock
SLP-76
SLP-76 K56E

SUPPLEMENTAL FIGURE LEGENDS

Figure S1: (A) SLP-76 binds to RanGAP1 and not to RanBP2, Related to Figure 1. Upper panel: SLP-76 binds to RanGAP1 co-expressed in 293T cells. 293T cells were transfected with control vector (lane 1) or SLP-76 WT (lane 2), subjected to immune precipitation with anti-RanGap1 and blotted for SLP-76 or RanGAP1. Anti-RanGAP1 co-precipitated SLP-76 (lane 2). Lower panel: SLP-76 does not bind to RanBP2 co-expressed in 293T cells. 293T cell lysates (left) and anti-RanBP2 immune precipitates (right) from mock control vector (lanes 1, 3) or GFP-RanBP2/HA-SLP-76 (lanes 2, 4). Transfectants were then blotted with anti-SLP-76 or anti-GFP. Anti-RanBP2 precipitated itself (lane 4-band lower than slight higher non-specific band in mock control) but not SLP-76 (lane 4) from GFP-RanBP2/HA-SLP-76 WT transfected cells. (B) SLP-76 binds to RanGAP1, but not to NFATc1. Jurkat cells were ligated with anti-CD3 for 10min (lanes 2,4,6) followed by immune precipitation using mIgG (lanes 1,2); anti-NFATc1 (lanes 3,4); anti-SLP-76 (lanes 5,6). While anti-CD3 increased RanGAP-1 co-precipitated by anti-SLP-76 (lane 6 vs. 5), anti-NFATc1 failed to precipitate SLP-76 (lanes 3,4) and vice versa (lane 5,6). Anti- NFATc1 also failed to co-precipitate RanGAP1 (lanes 3,4). (C) RanGAP1 in anti-SLP76 precipitates confirmed by MALDI-MS/MS spectrometry. Upper left panel: Colloidal Blue staining of proteins precipitated by anti-SLP-76 or isotope mouse IgG control from mouse T8.1 cells. Upper right panel: Blotting of anti-SLP-76 precipitates from quantitative isolation showing RanGAP1 and GADs. Middle box: List of SLP-76 interacting proteins identified in mouse T8.1 cells by mass spectrometry. Lower Box: List of RanGAP1 peptides identified in anti-SLP76 immune precipitates via LC-MS/MS analysis.

Figure S2: SLP-76 binding to RanGAP1 regulates exchange activity, Related to Figure 2. (A) Higher RanGAP1 exchange activity in anti-SLP-76 compared to anti-RanGAP1 precipitates. T8.1 cells were either incubated with IgG control or anti-CD3

for 5min followed by precipitation from lysates with mouse IgG, anti-SLP-76 or anti-RanGAP1. GTPase exchange activity involving Ran GTP hydrolysis was measured as in *Experimental Procedures*. Exchange activity was normalized relative to the amount of RanGAP1 precipitated by anti-SLP-76 or anti-RanGAP1 as detected by anti-RanGAP1 blotting. Background levels of activity associated with cells treated with the IgG control were then subtracted from values obtained from cells ligated with anti-CD3. The normalised activity in the anti-SLP-76 precipitates was then subtracted from the normalized activity in the anti-RanGAP1 precipitates to obtain the activity values for SLP-76 free RanGAP1. Upper panel: histogram showing normalized RanGAP1 exchange values. Lower panel: Western blotting showed RanGAP1 protein precipitated by anti-SLP-76 and anti-RanGAP1. Statistical significance by mean +/- SEM; *p<0.05, ; **p<0.01; ***p<0.001. (B) Lower exchange activity in anti-RanGAP1 precipitates from J14 cells expressing K56E versus wild-type SLP-76. SLP-76 deficient J14 T cells were transfected with SRα empty vector, HA tagged SLP-76 WT or the K56E mutant. 24 hours later, cells were stimulated with anti-CD3 for 10 minutes followed by cell lysis and precipitation with anti-RanGAP1. A measurement of *in vitro* RanGAP1 activity assay was the performed as in *Experimental Procedures*. Exchange activity was normalized relative to the amount of RanGAP1 precipitated by anti-RanGAP1. Upper panel: histogram showing normalized RanGAP1 exchange values. Lower panel: Western blotting showed RanGAP1 protein precipitated by anti-RanGAP1. Statistical significance by mean +/- SEM; *p<0.05, ; **p<0.01; ***p<0.001.

Figure S3. Calcium influx and NFAT nuclear entry, Related to Figure 3. (A) Calcium influx is similar in J14 cells expressing SLP-76 WT vs K56E mutant. SLP-76 deficient J14 cells transfected with vector control vs. pcDNA-SLP-76 WT or K56E mutant were subjected to calcium influx measurement with Indo-1. Calcium influx was monitored by flow cytometry at excitation wavelengths of 480 and 405 nm using

a Becton Dickinson CyAn cytometer. (B) Delineation of the nucleus vs. cytoplasm. Delineation of the nucleus vs. cytoplasm (dotted lines) showing that anti-CD3 induced NF-ATc1 nuclear translocation is impaired in J14 cells expressing K56E. J14 cells were co-transfected with NF-ATc1-GFP together with either HA-SLP-76 wild type or HA-SLP-76 K56E followed by anti-CD3 (2 μg/ml) ligation for 15 minutes, fixation with BD Cytofix/Cytoperm and staining with anti-HA (Alexa Fluor 633). Left panels show examples of NF-ATc1-GFP localization in transfected cells; right panels show examples of the cells with lines that delineate NF-ATc1-GFP localization in the cytoplasm and nucleus (i.e. based on DAPI staining).

Figure S4. SLP-76 and RanGAP1 synergize while binding is needed for optimal PMA/ionomycin induced NFAT activation, Related to Figure 4. (A) SLP-76 and RanGAP1 synergize to increase anti-CD3 induced NFAT1c driven transcription, and this effect is impaired by the K56E mutant. Jurkat J14 cells were co-transfected with the NFAT driven luciferase reporter together with SRα2 based expression constructs encoding empty vector as a control, HA-RanGAP1, HA-SLP-76 WT, HA-SLP-76-K56E, HA-SLP-76-WT/HA-RanGAP1 and HA-SLP-76 K56E/HA-RanGAP1. Cells were stimulated with 0.1ug/ml anti-CD3 followed by a measure of luciferase activity as described above. Left panel: histogram showing SLP-76 and RanGAP1 synergy and its reduction by K56E mutation. Upper inset: immune blot showing similar levels of transfected HA-tagged SLP-76 versus K56E expression in J14 cells relative to normal endogenous SLP-76 in parental Jurkat cells. Right panel: immune blot showing protein levels in lysates from transfected J14 cells for HA-SLP-76, HA-SLP-76 K56E and HA-RanGAP1. Data are means of +/- SD from a representative experiment (n=4). (B) Immunofluorescence staining pattern of SLP-76-YFP and mRFP-RanGAP1 in transfected T-cells. Jurkat T-cells were co-transfected with SLP-76-YFP and mRFP-RanGAP1 followed by 24 hours post-transfection, stimulated with

anti-CD3 (2μg/ml) for 15 mins, followed by incubation with BD Cytofix/Cytoperm fixation solution. (a): SLP-76-YFP; (b): mRFP-RanGAP1; (c): merged panel. Both SLP-76-YFP and mRFP-RanGAP1 are were localized to the cytoplasm. The intense insertional labeling corresponds to the Golgi region between lobes of the nucleus. (C) RanGAP1 binding to SLP-76 is needed for optimal PMA/ionomycin induced NFAT activation. J14 cells were co-transfected with SLP-76 (wild-type) or the K56E mutant plus a luciferase reporter construct carrying the NF-kB sequences from the interleukin 2 promoter. Cells were stimulated with PMA/ionomycin followed by harvesting of the cells and measurement of luciferase activity some 6 hours later. Data are means of +/- SD from a representative experiment (n=3). (D) SLP-76 K56E inhibits anti-CD3 induced IL-2 production as measured by intracellular staining. Pre-activated and rested primary mouse T-cells were transfected with mock (SRα vector), SLP-76 WT or SLP-76 K65E and left either untreated or activated with anti-CD3 (1 and 2ug/ml) for 24 hours prior to intracellular staining with anti-IL-2. Data are means of +/- SD from a representative experiment (n=4).

Movie S1: Real time movie of micro cluster formation at the interface of anti-CD3 (OKT3)-coated coverslips with SLP-76 WT-EYFP–transfected J14 (left panel) and SLP-76 K56E-EYFP–transfected J14 T cells (right panel). Related to Figure 3.

EXTENDED EXPERIMENTAL PROCEDURES

Cell culture and reagents

Jurkat T-cells, were obtained from the ATCC, while the SLP-76 deficient Jurkat J14 T- cells were a kind gift from A. Weiss, UCSF. Mouse hybridoma T8.1 is a murine T cell hybridoma expressing human CD4 and a chimeric human–mouse TCR specific for a tetanus toxin peptide (830–843) restricted by HLA-DRB1*1102 or HLA-DRB1*1301 (Blank et al., 1993)(a gift from O. Acuto, Oxford). DC27.10 cells

were originally derived from the mouse cell line DO-11.10 and is an L3T4 positive, Lyt-2,3-negative T cell hybridoma (Marrack et al., 1983) as has previously described in the lab (Liu et al., 2010; Raab et al., 1999; Schneider et al., 2008). Antibodies included anti-human CD3 (OKT3), hamster anti-mouse CD3 2C11 (ATCC), anti-SLP-76 (BioXcell, West Lebanon, NH), anti-RanGAP1 (Santa Cruz Biotechnology, Santa Cruz, CA, USA), Mab414 (Covance), anti-SUMO1 (a gift from R. Hay, Dundee, UK), anti-Carma1 (Cell Signaling, Danvers, MA), anti-HA (Covance), anti-Lck, anti-ADAP, anti-SKAP1 and anti-GADS (Upstate Biotechnology, Lake Placid, NY), anti-NF-ATc1 (Santa Cruz Biotechnology, Santa Cruz, CA, USA), anti-RanBP2 (Thermo scientific); Monoclonal antibody against nuclear pore complex Mab414 (Covance), anti-actin (Sigma-Aldrich, Inc., St. Louis, OM, USA). CFSE (carboxyfluorescein diacetate succinimidyl ester) was purchased from Sigma (Poole, UK)

Expression vectors and plasmids

SLP-76-HA was constructed by sub-cloning SLP-76 cDNA into the *Xba*I /*Kpn*I sites of SRα2 vector or into the *Xba*I /*Kpn*I sites of pCDNA3.1(-) vector with N-terminally 2XHA tags. RanGAPRanGAPHA tagged RanGAP1 was constructed by sub-cloning human RanGAP1 cDNA into the *Xba*I/*Kpn*I sites of SRα2 vector. mRFP-RanGAP1 was constructed by sub-cloning human RanGAP1 cDNA into the *Bgl*II/*Hin*dIII sites of pMaxFp-red C1 vector (Amaxa). For SLP-76-YFP fusion construct, the human SLP-76 cDNA was amplified by PCR and was subcloned into the *Xho*I/*Bam*HI sites of pEYFP-N1 vector (Clontech). The constructs coding for K56E SLP-76 mutant fused to HA and EYFP were generated by point mutations of lysine to glutamic acid using a site-directed QuikChange mutagenesis kit (Stratagene) with primers: 5′- gacatccaggagttccccaagctccgggtg -3′ and 5′-cacccggagcttggggaactcctggatgtc-3′. The pcDNA based NFATc1 with C-terminally

GFP fusion construct was a kind gift from M. Purbhoo, London. The GFP-RelA/p65 construct was purchased from addgene (Cambridge, MA, USA).

Transfection and stimulation

Jurkat and J14 T -cells were transfected by microporation (Digital Bio Technology), using a single pulse of 30 ms at 1410 V, and mouse DC27.10 cells with 2 pluses of 20 ms at 1400 V. To activate Jurkat cells, 5 x 10^6 cells were incubated with pre-warmed RPMI 1640 media supplemented with 2% FCS with either 2 µg/ml rabbit anti-mouse antibody or 2-5µg/ml of 145-2C11 (anti-CD3e) plus 2 µg/ml rabbit anti-mouse antibody at 37^{o}C for varying lengths of time. Peripheral blood human lymphocytes were isolated from buffy-coats by density gradient centrifugation and stimulated using the same regime. Human primary T -cells were transfected using a single pulse of 20 ms at 2259 V. To activate DC27.10 T cells, cells in in log growth phase were pelleted by centrifugation (1500 rpm for 5 mins) and suspended in serum free RPMI medium. Cells were then either incubated with an Ig isotope (2µg/ml), or stimulated with 2C11(2 µg/ml) at 37^{o}C for various times. Primary naïve mouse cells were transfected with various vectors using the Amaxa Nucleofector Kit (Lonza, Germany) according to the manufacturer's instructions and stimulated using the same regime as outlined for DC27.10 cells.

RanGAP1 GAP activity assays

The *in vitro* RanGAP1 GAP activity was measured by both radioactive and non radioactive assays. Isotype labelling is shown in Figs 2B and Fig. S2A, while the non-radioactive protocol was used in Figure S2B. For radioactive labelling, 2.5µg of human recombinant Ran (Sigma-Aldrich) was loaded with either cold GTP (15 mM) or [γ-^{32}P] GTP (15 Ci/mm, PerkinElmer) in the presence of loading buffer (10 mM EDTA, 2 mM ATP, 4 mM DTT, and 50 mM HEPES, pH 7.4) in 150 µl. Loading mixture was incubated at room temperature for 30min, then diluted 10-fold into buffer

(5 mM $MgCl_2$, 1 mM DTT, 0.1 mg/ml BSA, 0.005% Tween 20, and 50 mM HEPES, pH 7.4). Unbound GTP was removed on a NAP-5 column (GE Healthcare) and eluted with 1 mL GAP buffer (20 mM Tris-HCl pH 8.0, 50 mM NaCl, 5 Mm $MgCl_2$, 0.05% BSA). RanGAP activity, which measures RanGTP hydrolysis, was then quantified using either a Phos-Free Phosphate Assay Kit (Cytoskeleton Inc., Denver, CO) according to manufactory's protocol or isotope labelled *in vitro* RanGAP1 GAP activity assay as described (Bischoff et al., 1994). For a measurement of activity in precipitates, 40 μl of 60 nM Ran [γ^{32}P] GTP (pre-loaded *in vitro*) was added to a volume of 10 μl of precipitate and incubated at 37°C. The GTPase reaction was stopped by addition of 1 ml of charcoal suspension [7% charcoal/10% ethanol/0.1 M HCl/10 mM KH_2PO4]. After centrifugation at 10,000xg, the release of [γ^{32}P] phosphate was determined in a liquid scintillation counter. Values associated with protein A beads in the absence of antibody was subtracted from values associated with anti-SLP-76 or RanGAP1 precipitates.

In the non radioactive assay, the release of free phosphate was measured as an increased in absorbance at 650 nm. RanGAP activity, which measures RanGTP hydrolysis, was then quantified using either a Phos-Free Phosphate Assay Kit (Cytoskeleton Inc., Denver, CO) according to manufactory's protocol. Quantitation was based on the relative intensities of RanGAP1 in blots under conditions of non-saturated exposures. **p<0.01, ***p<0.001 vs SLP-76 WT. The average results were shown from three independent experiments.

Nuclear pore fraction isolation

Nuclear pore fractions were separated from cytoplasmic fractions of mouse hybridoma DC27.10 T -cells by using the Thermo NE-PER Nuclear and Cytoplasmic Extraction Kit (Fischer scientific). This involved a stepwise lysis of cells and centrifugal isolation of nuclear and cytoplasmic protein fractions. The nuclear extract

and nuclear envelope fraction containing nuclear pore complex were then extracted as previously described (Florens et al., 2008).

Immune precipitation and blotting

Immunoprecipitation and blotting were preformed as previously described (Raab et al., 2011). Briefly, Jurkat, primary mouse or human T-cells were harvested and lysed with lysis buffer (20mM Tris-HCl, pH 8.0, 150mM NaCl, 1% (v/v) Triton X-100, 1 mM phenylmethylsulfonyl fluoride, 1 mM Na_3VO_4, 1mM NaF, 1mM leupeptin, 1mM pepstatin, and 1% aprotinin). Immunoprecipitation was carried out by incubation of the lysate with the antibody for 1 h at 4 °C, followed by incubation with 30 μl of protein A/G-agarose beads (50% w/v) for 1 h at 4 °C. For immune blotting, the immunoprecipitates were separated by SDS-PAGE and transferred onto nitrocellulose filters (Schleicher and Schuell). Filters were blocked with 5% (w/v) skimmed milk for 1 h in Tris-buffered saline pH 8.0 and then probed with the indicated primary antibody. Bound antibody was revealed with horseradish peroxidase conjugated corresponding secondary antibody using enhanced chemiluminescence (ECL, Amersham Biosciences).

Liquid chromatography tandem mass spectrometry (LC-MS/MS)

For LC-MS/MS (conducted by Cambridge Centre for Proteomics, Cambridge University), identification of SLP-76 associated proteins was made by peptide mass fingerprinting using trypsin digestion and a MALDI mass spectrometer. Anti-SLP-76 was precipitated from DC27.10 or T8.1 T-cells that had been stimulated for 24 hours with anti-CD3 (2C11) prior to detergent solubilisation. Gels were stained with colloidal on thin mini-gels to minimise the volume of gel and solutions were carefully filtered prior to use, wearing gloves at all times. After staining/destaining, image gels were washed in 10% (v/v) methanol to remove acid, gel bands were excised and subjected to the following treatment (30min per step, 20^{o}C, in 200µl 100mM

ammonium bicarbonate/50% acetonitrile). This included reduction with 5mM tris(2-carboxyethyl)phosphine, alkylation by addition of iodoacetamide (25mM final concentration.) and digestion for 17h at 32^{o}C in 25µl 100mM ammonium bicarbonate containing 5µg/ml modified trypsin (Promega). Peptides were then desalted using µC18 ZipTip (MIllipore) and eluted to a MALDI target plate using 1.5µl alpha-cyano-4-hydroxycinnamic acid matrix (Sigma) in 50% acetonitrile/0.1% trifluoroacetic acid. Peptide masses were determined using a Maldi micro MX mass spectrometer (Waters) and analysed with Masslynx software. Database searches of the mass fingerprint data were performed using Mascot (http://www.matrixscience.com). For tandem ms/ms analysis, desalted peptides in were delivered to a ThermoFinnigan LCQ Classic ion-trap mass spectrometer using a static nanospray needle (Thermo Proxeon). Fragment ions were matched to possible sequence interpretations using MS-Product and/or MS-Tag (http://prospector.ucsf.edu/).

Immunofluorescence and Confocal Imaging

Cells were harvested, washed in PBS and fixed in Cytofix (BD Bioscience) for 30min at 4°C. Cells were then permeabilized in PBS containing 0.5% Saponin and 1% bovine serum albumin (BSA) for 90min with primary antibody for 1 h. Cells were then washed in PBS containing 0.1% Saponin and 1% BSA and incubated with fluorescently labeled secondary antibody for 1h. Incubation and washing for subsequent primary and secondary antibodies were repeated for double and triple-stained cells. After the final wash, cells were re-suspended in Vectashield mounting medium containing DAPI (4,6-diamidino-2-phenylindole; Vector Laboratories), mounted onto microscope slides, and sealed with nail varnish. Further live cell imaging on poly-L-lysine (Sigma) and anti-CD3 -treated cover slides (LabTek, Rochester, NY) was conducted as described (Bunnell et al., 2002; Bunnell et al., 2006; Liu et al., 2010; Purbhoo et al., 2010). .

For staining of SLP-76 at the nuclear pore complex, mouse DC27.10 T -cells were either left untreated or stimulated with soluble anti-CD3 at 2 μg/ml or the same concentration of hamster IgG as a control. Sequential immunofluorescence staining was then performed using primary antibodies, anti-SLP-76 (mouse IgG1) and anti-RanGAP1 (rabbit IgG) or MAb 414 (mouse IgG1). Cells were then washed in PBS at 4^{o}C followed by staining using secondary antibodies Alexa Fluor 488 conjugated anti-mouse IgG, and Alexa Fluor 488 conjugated anti-rabbit IgG (Invitrogen) or anti-mouse IgG1 murine coupled Alexa Fluor 633. DAPI was used to stain the nuclei.

For imaging of NFATc1-EGFP, J14 cells were co-transfected with NF-ATc1-GFP together with either HA-SLP-76 WT or HA-SLP-76 K56E. 24 hours post-transfection, the cells were either mock-treated or stimulated with anti-CD3 (2 μg/ml) for 15min, followed by incubation with BD Cytofix/Cytoperm fixation solution supplemented with DAPI, and staining with anti-HA (Alexa Fluor 633). The fluorescence intensity of NF-ATc1-GFP in the whole cell region (red dashed line circled) and in the nuclear region (the white dashed line circled) was quantified using the Image J program, from which the percentages of nuclear NF-ATc1-EGFP were calculated. Quantification of nuclear/total for NFATc1-EGFP was carried out for T -cells either expressing SLP-76 WT or K56E mutant with or without anti-CD3 stimulation.

Image acquisition was performed with a Zeiss LSM510 confocal microscope using a 63 Plan Apochromat/1.4- numerical-aperture oil objective lens. Lasers of 405-nm (DAPI)-, 488-nm (GFP and Alexa Fluor 488)-, 514-nm (EYFP), 594-nm (mRFP) and 633-nm (Alexa Fluor 647) wavelengths were used for fluorescence excitation. Images were processed with Leica confocal software (LCS; Leica Microsytems), Volocity (Improvision), and ImageJ (National Institutes of Health).

For imaging NFκB nuclear translocation, J14 cells were co-transfected with GFP-RelA/p65 together with either HA-SLP-76 WT or HA-SLP76 K56E mutant. 24

hours post-transfection, cells were either left untreated or stimulated with anti-CD3 (2μg /ml) for 5 and 15 min. Cells were washed and fixed with 4% paraformaldehyde) for 30 min. After permeabilization with 0.5% Saponin for 30 min, cells were washed and incubated with anti-HA antibody followed by Alexa Fluor 633 for 1 hour, respectively. After the final wash, cells were resuspended in Vectashield mounting medium containing DAPI (Vector Laboratories). Image acquisition was performed with a Zeiss LSM700 confocal microscope.

***In vivo* adoptive T-cell transfer assay**

For *in vivo* experiments, DO11.10 T-cells were isolated by using a mouse T-cell enrichment column kit (R&D, Abingdon, UK). DO11.10 T-cells were stimulated with anti-CD3 (2μg/ml) and anti-CD28 (5μg/ml) antibodies. The cells were pre-activated for 72 hours and then rested for 24 hours and were transfected with HA-SLP-76 or HA-SLP-76 K53E, labeled with CFSE (5μM). Cells were transfected with empty vector (mock), SLP-76 WT or SLP76 K56E using the Amaxa Nucleofector Kit (Lonza, Germany) (routinely gave up to 50-60% uptake efficiency). Transfected cells were labelled with CFSE and injected i.v. into the tail of Balb/c mice ($4x10^6$ cells) followed by iv injection of 50μgOVA peptide 24 hours later. Proliferation of CFSE labelled T-cells was assessed 6 days after the OVA-peptide injections by FACs analysis.

Transmission electron microscopy (TEM)

Log growth phase DC27.10 T-cells with or without anti-CD3 stimulation (1 μg/ml for 10min) were fixed by adding 1:1 double-strength fixative solution (8% PFA in 0.2 M phosphate buffer pH 7.4) to the culture medium for 5min followed by 2h in fresh 4% PFA in 0.2 M phosphate buffer pH 7.4 (Richardson and Leitch, 2007). Cells were then pelleted in 10% gelatin, infiltrated with 2.3 M sucrose and then frozen by

plunging into liquid nitrogen (Richardson and Leitch 2007). Frozen pellets were sectioned on a cryo-ultramicrotome (Leica, UC6 with FC6 cryo-attachment). Cryosections were thawed, rinsed in PBS with 1% glycine, incubated in PBS with 1% BSA, incubated with anti SLP76 antibody at a dilution of 1:50, rinsed in PBS and then incubated in secondary anti-mouse IgG antibody conjugated to 5 nm colloidal gold (Agar Scientific, UK). Alternatively anti-RanGAP was used at 1:400 to 1:2000 dilutions. Grids were then rinsed in PBS, transferred to 1% glutaraldehyde (Agar Scientific, UK) in PBS, washed in water and embedded in 2% methyl cellulose containing 0.4% uranyl acetate (Agar Scientific, UK). Images were taken on a Hitachi H7600 electron microscope. In order to measure the distances, since the cytoplasmic ring could not be directly visualised, first the distance from the central plane to the particle was measured, then the known distance (40 nm) from the central plane to the top of the cytoplasmic ring (Maimon et al., 2012) was subtracted to give the ring-label distance.

Measurement of intracellular calcium

SLP-76 deficient J14 cells transfected with pcDNA-SLP-76 WT or K56E mutant were subjected to calcium influx measurement (Parry et al., 2000). Briefly, cells were incubated at a density of 2×10^6 cells/ml in RPMI 1640, 1% FCS, and 5 μM Indo-1 (Invitrogen) for 1 h before being washed twice in HBSS and re-suspended at 10^5 cells/ml in HBSS/0.2% FCS. After the addition of 2μg/ml anti-CD3 antibody or 1 μg/ml ionomycin as a positive control, calcium influx was monitored by flow cytometry at excitation wavelengths of 480 and 405 nm using a Becton Dickinson CyAn cytometer. A total of 2 μg/ml ionomycin (Sigma-Aldrich) served to elicit the maximum response while the relative concentration of intracellular free Ca^{2+} was measured as the median fluorescence ratio of Indo-1 bound/unbound (405/485 nm) over time. For statistical comparisons, the calcium response was normalized and expressed as the ratio of the maximum peak post-stimulation to baseline. Kinetic

plots were generated on ligated (Indo-1–labeled) cells using FlowJo software.

Promoter Reporter Assays and Intracellular FACs Staining

For the IL-2 NFAT luciferase reporter construct, Jurkat or J14 T-cells were transfected with an IL-2 promoter reporter vector (3 copies of NFAT binding sites and control vector (Promega, Madison, WI). 18 hours post-transfection, cells were either incubated with IgG isotype control or stimulated with various concentrations of anti-CD3 (0.1-1μg/ml anti-CD3) at 37 °C for 6 h and subsequently assayed for luciferase activity using a luminometer (MicroLumat, EG&G Berthold). Luciferase units of the experimental vector were normalized to the level of the control vector in each sample.

For the IL-2 NF-kB luciferase (firefly) reporter plasmid, T-cells were transfected with the reporter plasmid together with Renilla luciferase plasmid (pRLTK, Promega) as an internal control to adjust for the transfection efficiency and background. Following 24 hours of expression, cells were ligated with anti-CD3 for six hours. Cells were then lysed in 100μl of lysis buffer of the dual luciferase assay kit (Promega). Light units were recorded on Luminometer (Berthold) from 10μl of sample in 100μl substrate solution as per the manufacturer's instructions. All the relative luciferase units (RLU) were derived by normalizing relative to internal Renilla values.

For intracellular FACs staining, primary murine T-cells were activated with anti-CD3 (5μg/ml) and anti-CD28 (5μg/ml) for 72 hours. Cells were then washed and after 24 hours transfected with Mock, SLP-76 WT and SLP-76-K56E mutant using the Amaxa Nucleofector Kit. 24 hours after transfection, cells were either left unstimulated or activated with plate-bound anti-CD3 (1 and 2μg/ml) for 48 hours. Brefeldin A was added 6 hours before fixation with 4% (v/v) paraformaldehyde. After

permeabilization with 0.5% (w/v) Saponin, the cells were stained with-phycoerythrin labeled anti-IL-2 and analyzed by FACS.

Bischoff, F.R., Klebe, C., Kretschmer, J., Wittinghofer, A., and Ponstingl, H. (1994). RanGAP1 induces GTPase activity of nuclear Ras-related Ran. Proc Natl Acad Sci U S A *91*, 2587-2591.

Blank, U., Boitel, B., Mege, D., Ermonval, M., and Acuto, O. (1993). Analysis of tetanus toxin peptide/DR recognition by human T cell receptors reconstituted into a murine T cell hybridoma. Eur J Immunol *23*, 3057-3065.

Bunnell, S.C., Hong, D.I., Kardon, J.R., Yamazaki, T., McGlade, C.J., Barr, V.A., and Samelson, L.E. (2002). T cell receptor ligation induces the formation of dynamically regulated signaling assemblies. The Journal of cell biology *158*, 1263-1275.

Bunnell, S.C., Singer, A.L., Hong, D.I., Jacque, B.H., Jordan, M.S., Seminario, M.C., Barr, V.A., Koretzky, G.A., and Samelson, L.E. (2006). Persistence of cooperatively stabilized signaling clusters drives T-cell activation. Mol Cell Biol *26*, 7155-7166.

Florens, L., Korfali, N., and Schirmer, E.C. (2008). Subcellular fractionation and proteomics of nuclear envelopes. Methods Mol Biol *432*, 117-137.

Liu, H., Purbhoo, M.A., Davis, D.M., and Rudd, C.E. (2010). SH2 domain containing leukocyte phosphoprotein of 76-kDa (SLP-76) feedback regulation of ZAP-70 microclustering. Proc Natl Acad Sci U S A *107*, 10166-10171.

Maimon, T., Elad, N., Dahan, I., and Medalia, O. (2012). The human nuclear pore complex as revealed by cryo-electron tomography. Structure *20*, 998-1006.

Marrack, P., Shimonkevitz, R., Hannum, C., Haskins, K., and Kappler, J. (1983). The major histocompatibility complex-restricted antigen receptor on T cells. IV. An antiidiotypic antibody predicts both antigen and I-specificity. J Exp Med *158*, 1635-1646.

Parry, C.M., Simas, J.P., Smith, V.P., Stewart, C.A., Minson, A.C., Efstathiou, S., and Alcami, A. (2000). A broad spectrum secreted chemokine binding protein encoded by a herpesvirus. J Exp Med *191*, 573-578.

Purbhoo, M.A., Liu, H., Oddos, S., Owen, D.M., Neil, M.A., Pageon, S.V., French, P.M., Rudd, C.E., and Davis, D.M. (2010). Dynamics of subsynaptic vesicles and surface microclusters at the immunological synapse. Science signaling *3*, ra36.

Raab, M., Kang, H., da Silva, A., Zhu, X., and Rudd, C.E. (1999). FYN-T-FYB-SLP-76 interactions define a T-cell receptor zeta/CD3-mediated tyrosine phosphorylation pathway that up-regulates interleukin 2 transcription in T-cells. J Biol Chem *274*, 21170-21179.

Raab, M., Smith, X., Matthes, Y., Strebhardt, K., and Rudd, C.E. (2011). SKAP1 PH domain determines RAPL membrane localization and Rap1 complex formation for TCR activation of LFA-1. J Biol Chem *2011*, 29663-70286.

Richardson, C.A., and Leitch, B. (2007). Identification of the neurotransmitters involved in modulation of transmitter release from the central terminals of the locust wing hinge stretch receptor. . Journal of Comparative Neurology *502*, 794-80.

Schneider, H., Smith, X., Liu, H., Bismuth, G., and Rudd, C.E. (2008). CTLA-4 disrupts ZAP70 microcluster formation with reduced T cell/APC dwell times and calcium mobilization. Eur J Immunol *38*, 40-47.